Vibrational Absorption and Circular Dichroism of Mono- and Dimethyl Derivatives of 6,8-Dioxabicyclo[3.2.1]octane

C. S. Ashvar,[†] F. J. Devlin,[†] P. J. Stephens,*[,†] K. L. Bak,[‡] T. Eggimann,[§] and H. Wieser[§]

Department of Chemistry, University of Southern California, Los Angeles, California 90089-0482, UNI-C, Olof Palmes Allé 38, DK-8200 Aarhus N, Denmark, and Department of Chemistry, University of Calgary, Calgary, Alberta, Canada T2N 1N4

Received: March 24, 1998; In Final Form: June 11, 1998

Ab initio density functional theory (DFT) is used to analyze the vibrational unpolarized absorption and circular dichroism spectra (below 1500 cm^{-1}) of seven derivatives of 6,8-dioxabicyclo[3.2.1]octane. Two are methyl derivatives, two are methyl-d_3 derivatives, and three are dimethyl derivatives. DFT calculations use hybrid functionals (B3LYP and B3PW91), the 6-31G* basis set, and, in predicting circular dichroism spectra, GIAO basis sets. The two functionals give qualitatively similar spectra. Comparison of predicted and experimental spectra permits assignment of the majority of the fundamentals of the seven molecules (excluding C−H stretching modes). Vibrational circular dichroism intensities are in good overall agreement with experiment, consistent with previously assigned absolute configurations. Spectra are also predicted using the Hartree−Fock/self-consistent field (HF/SCF) and MP2 methodologies. MP2 spectra are similar in accuracy to DFT spectra. HF/SCF spectra are of much lower accuracy and are in poor agreement with experiment.

Introduction

We report studies of the vibrational unpolarized absorption (IR) and the vibrational circular dichroism (VCD) spectra of five derivatives of the chiral molecule 6,8-dioxabicyclo[3.2.1] octane (**1**). Two are monomethyl derivatives: *exo*-7-methyl-**1** (**2**) and *endo*-7-methyl-**1** (**3**). Three are dimethyl derivatives: *exo*-5,7-dimethyl-**1** (**4**), *endo*-5,7-dimethyl-**1** (**5**), and 1,5-dimethyl-**1** (**6**). One, **6**, is a naturally occurring insect pheromone, frontalin.[1] The structures of **1**−**6** are displayed in Figure 1. In addition, we have studied the unpolarized absorption spectra of the methyl-d_3 derivatives of **2** and **3**: **7** and **8**.

Theoretical analysis of the experimental spectra of **2**−**8** is carried out using *ab initio* density functional theory (DFT).[2] As a result of the implementation of analytical derivative methods for calculating energy second derivatives,[3] DFT is increasingly used in analyzing vibrational unpolarized absorption spectra. Recent developments now permit VCD spectra to be predicted using DFT at the same level of accuracy.[4−8] DFT analysis of the absorption and VCD spectra of **1** was recently reported.[5] This work is here extended to the derivatives, **2**−**8**.

Our goals are as follows: (1) to assign the vibrational spectra of **2**−**8** in the fundamental vibrational region (excluding the C−H stretching region); (2) to examine the predictive capabilities of DFT at the 6-31G* basis set level and using hybrid functionals[9] with regard to fundamental vibrational frequencies, absorption intensities, and circular dichroism intensities; (3) to compare the accuracies of two state-of-the-art hybrid functionals, B3LYP and B3PW91;[10] (4) to compare DFT vibrational spectra to spectra predicted using Hartree−Fock/self-consistent field (HF/SCF) and MP2 methodologies; and (5) to confirm the absolute configurations of **2**−**6** arrived at previously.[11]

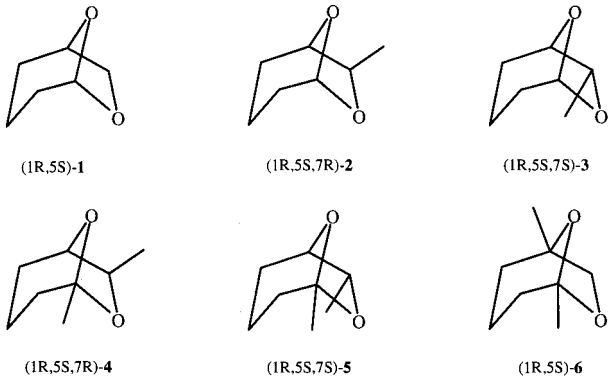

Figure 1. Structures of **1**−**6**.

Methods

Racemic and optically active **2**−**6** were obtained as described by Ibrahim et al.[11] All racemic compounds were obtained by chemical synthesis. Single enantiomers of **2**−**5** were obtained using enzymatic methods; enantiomers of **6** were obtained via chemical synthesis. Chemical purities of all compounds and absolute configurations and optical purities of optically active compounds used in this work are listed in Table 1. Racemic **7** and **8** were obtained by straightforward modifications of the synthetic routes for **2** and **3**.

Unpolarized absorption spectra were measured for solutions of racemic **2**−**8** over the range 400−1500 cm^{-1} at 1 cm^{-1} resolution using a Nicolet 8000 FTIR spectrometer. Solvents were CS_2 (700−840 cm^{-1}) and CCl_4 (<700 and >840 cm^{-1}), concentrations were 0.3−0.6 M, and cell path length was 100 μm. VCD spectra of **2**−**6** were measured over the range 800−1500 cm^{-1} at 4 cm^{-1} resolution using the Nicolet 8000 VCD accessory described previously.[12] All VCD spectra were obtained using single enantiomers; solvent baseline spectra were subtracted. The solvent was CCl_4, concentrations were 0.05−

* To whom correspondence should be addressed.
[†] University of Southern California.
[‡] UNI-C.
[§] University of Calgary.

S1089-5639(98)01602-8 CCC: $15.00
Published on Web 07/29/1998

TABLE 1: Derivatives of 1

compound[a]	enantiomer[a]	synthesis[b]	$[\alpha]_D$ (deg)	optical purity[c] (%)	chemical purity (%)
2	(±)	chem			>98
2	(−)-1*S*,5*R*,7*S*	enz	−93.5 (CCl_4)	99	87
3	(±)	chem			>98
3	(+)−1*R*,5*S*,7*S*	enz	+107.0 (CCl_4)	99	99
4	(±)	chem			>98
4	(−)-1*S*,5*R*,7*S*	enz	−65.6 ($CHCl_3$)	99	100
5	(±)	chem			>98
5	(+)−1*R*,5*S*,7*S*	enz	+86.5 ($CHCl_3$)	100	98
6	(±)	chem			>97
6	(+)−1*R*,5*S*	chem	+54.1 (c 4.5, ether)	95	>98
7	(±)	chem			
8	(±)	chem			

[a] See Figure 1 for structures and absolute configurations of **2**−**6**. [b] Chem stands for chemical synthesis; enz stands for enzymatic synthesis using baker's yeast.[11,13] [c] Obtained using chiral complexation gas chromatography.[11,13]

0.8 M, and cell pathlength was 100 μm. In addition, Raman spectra of molten liquid **2**, **3**, **7**, and **8** were measured, as described in detail elsewhere.[13] Portions of absorption spectra were subjected to Fourier self-deconvolution in order to increase the resolution of overlapping bands. Frequencies and dipole strengths for **2**, **3**, **7**, and **8** were obtained from absorption spectra by Lorentzian fitting.

Vibrational frequencies, dipole strengths, and rotational strengths were calculated within the harmonic approximation, as described previously.[4,5,7,8,14,15] DFT calculations were carried out using the GAUSSIAN program.[16] Atomic axial tensors (AATs) were calculated using gauge-invariant (including) atomic orbitals (GIAOs).[4,14] The two hybrid functionals used are the original hybrid functional of Becke,[9,10] B3PW91, and a widely used alternative functional of the same class, B3LYP.[10] HF/SCF calculations were carried out using the GAUSSIAN and SIRIUS/ABACUS[14,15,17] programs. Harmonic force fields (HFFs) and atomic polar tensors (APTs) were calculated using GAUSSIAN. AATs were calculated using GIAOs and SIRIUS/ABACUS. MP2 calculations were carried out using GAUSSIAN and SIRIUS/ABACUS. HFFs and APTs were calculated using GAUSSIAN. AATs were "semi-MP2" distributed origin gauge AATs; "local" AATs were calculated at the HF/SCF level using GIAOs and SIRIUS/ABACUS.[15] All ab initio calculations used analytical derivative methods. The 6-31G* basis set was used for the majority of the calculations. In the case of one molecule, **3**, calculations were also carried out using a much larger basis set: TZ2P, [5s4p2d/3s2p].[18] Unpolarized absorption and VCD spectra are obtained from calculated frequencies, dipole strengths, and rotational strengths, assuming Lorentzian band shapes.[19]

Results

The absorption spectra of CCl_4 and CS_2 solutions of **2**−**8** were measured over the range 400−1500 cm^{-1}; the spectra above 800 cm^{-1} are shown in Figures 2−8. Frequencies and dipole strengths obtained from the spectra are given in Tables 2−8. Gas-phase frequencies for **2**, **3**, **7**, and **8** in the range 0−400 cm^{-1}, obtained previously,[13,20] are also given in Tables 2, 3, 7, and 8.

Frequencies and dipole strengths predicted using DFT, 6-31G*, and the functionals B3LYP and B3PW91 are given in Tables 2−8. Absorption spectra predicted thence (using Lorentzian band shapes and a constant bandwidth) are shown in Figures 2−8 for the range 800−1600 cm^{-1}.

For each molecule, the B3PW91 and B3LYP absorption spectra are qualitatively very similar. Both functionals predict spectra in excellent overall agreement with experiment, permitting straightforward assignment of the majority of fundamentals in the range 0−1500 cm^{-1}. Assignment is most complex in the region 1300−1500 cm^{-1}, where the density of bands is greatest and the resolution of bands the least. Our assignments are given in Tables 2−8 and, for those modes above 800 cm^{-1}, in Figures 2−8.

***exo*-7-Methyl-6,8-dioxabicyclo[3.2.1]octane (2).** Modes 1−33 are straightforwardly assignable in the range 0−1300 cm^{-1}. Mode 31 is barely detectable in the IR spectrum but is more prominent in the Raman spectrum.[13] Above 1300 cm^{-1}, the number of bands exceeds the number of fundamentals and, in the cases of modes 34, 36, and 44, alternative assignments exist, as detailed in Table 2.

B3PW91 and B3LYP calculations yield very similar spectra and identical assignments. The largest differences in predicted spectra are for modes 22−27.

***endo*-7-Methyl-6,8-dioxabicyclo[3.2.1]octane (3).** Modes 1, 4, 7−24, and 27−33 are straightforwardly assignable in the range 0−1320 cm^{-1}. Modes 11 and 31 are very weak in the IR spectrum but are also observable in the Raman spectrum.[13] Modes 2/3, 5/6, and 25/26 are not resolved. Above 1320 cm^{-1}, the spectrum is more complex. Alternative assignments exist for modes 34 and 35 (Table 3). The band at 1457 cm^{-1} is either assignable to mode 44 alone or to both modes 43 and 44.

B3PW91 and B3LYP calculations yield very similar spectra and identical assignments. In the case of modes 25 and 26, very different relative intensities are predicted; however, these modes are not resolved.

***exo*-5,7-Dimethyl-6,8-dioxabicyclo[3.2.1]octane (4).** Modes 18−38 are straightforwardly assignable in the range 800−1300 cm^{-1}. Above 1300 cm^{-1}, the spectrum is more complex. Of modes 39−52, only modes 41 and 43 are resolved.

B3PW91 and B3LYP calculations yield very similar spectra and identical assignments. The relative intensities of modes 25/26 and 35/36 differ substantially; in each case, the observed ratio is intermediate between those predicted by the two functionals.

***endo*-5,7-Dimethyl-6,8-dioxabicyclo[3.2.1]octane (5).** In the range 800−1300 cm^{-1}, modes 18−20, 23−32, 35, and 36 are resolved; modes 21/22 and 33/34 are unresolved. Above 1300 cm^{-1}, modes 39, 42−45, 51, and 52 are resolved; modes 37/38, 40/41, 46/47, and 48−50 are unresolved.

B3LYP and B3PW91 calculations yield very similar spectra and identical assignments.

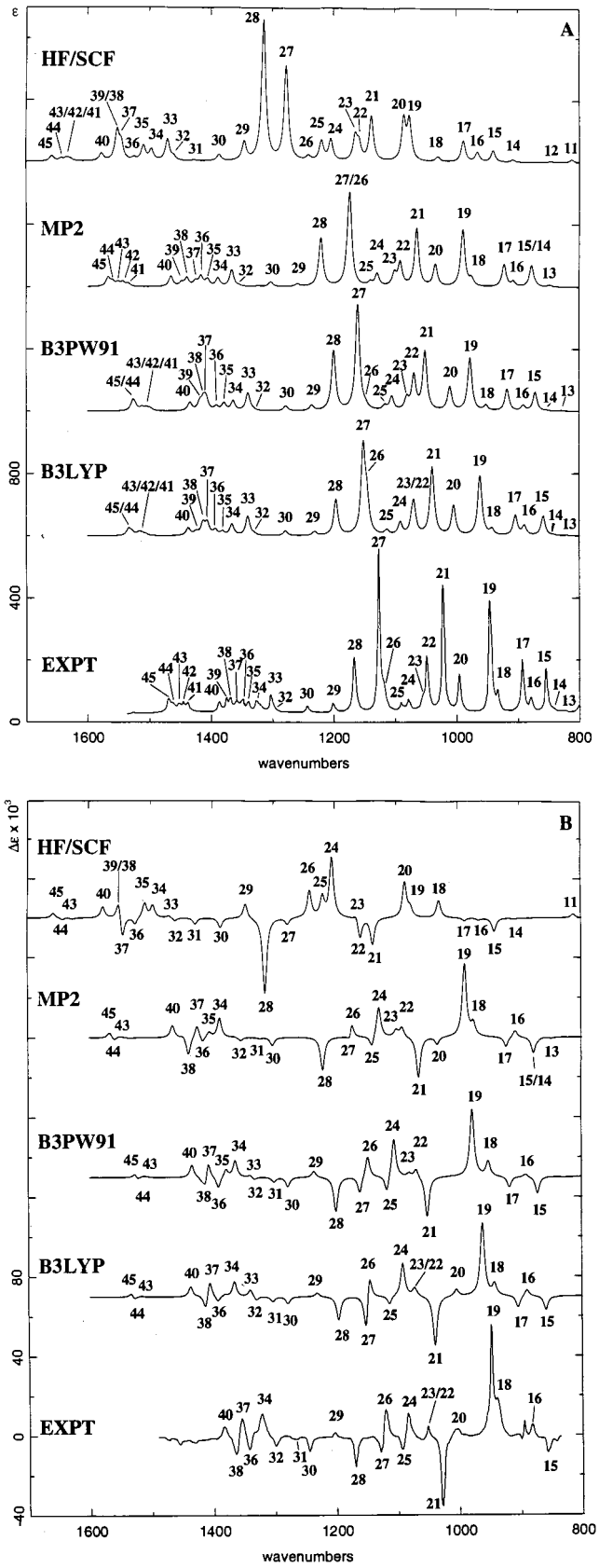

Figure 2. (A) Unpolarized absorption and (B) VCD spectra of **2**. Fundamentals are numbered. Calculated spectra use Lorentzian band shapes ($\gamma = 4.0$ cm^{-1}).

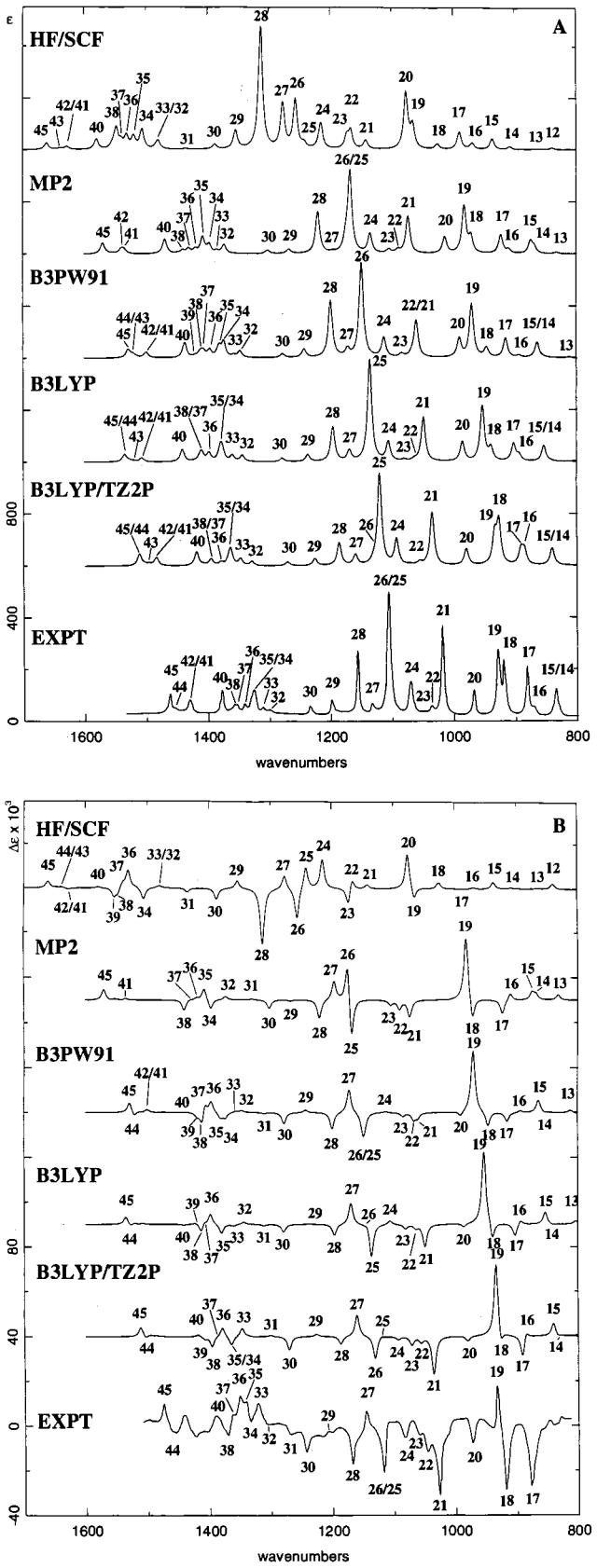

Figure 3. (A) Unpolarized absorption and (B) VCD spectra of **3**. Fundamentals are numbered. Calculated spectra use Lorentzian band shapes ($\gamma = 4.0$ cm^{-1}).

1,5-Dimethyl-6,8-dioxabicyclo[3.2.1]octane (6). In the range 800−1300 cm^{-1}, modes 18, 21−25, 29−32, and 35−38 are resolved; modes 19/20, 27/28, and 33/34 are unresolved. Mode 26 is not clearly identifiable. Above 1300 cm^{-1}, modes 39, 42−44, and 52 are resolved; modes 40/41, 45/46, 47−49, and 50/51 are unresolved.

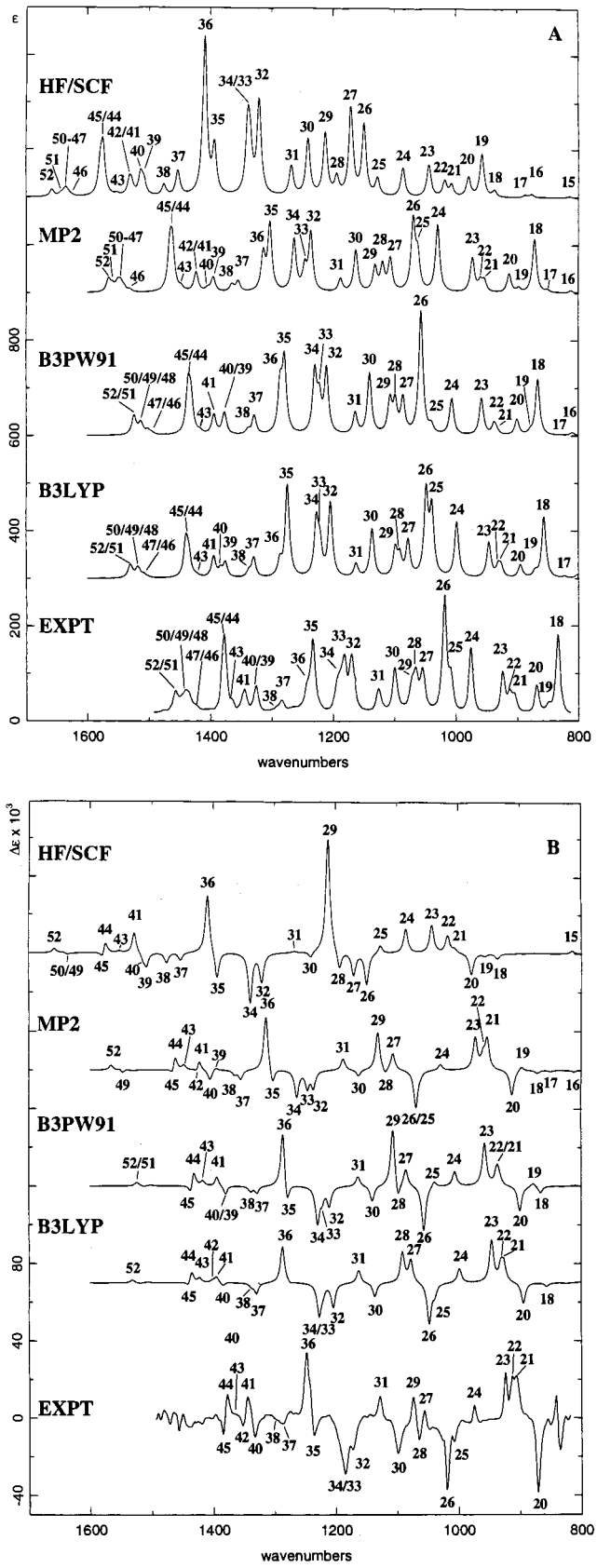

Figure 4. (A) Unpolarized absorption and (B) VCD spectra of **4**. Fundamentals are numbered. Calculated spectra use Lorentzian band shapes ($\gamma = 4.0$ cm^{-1}).

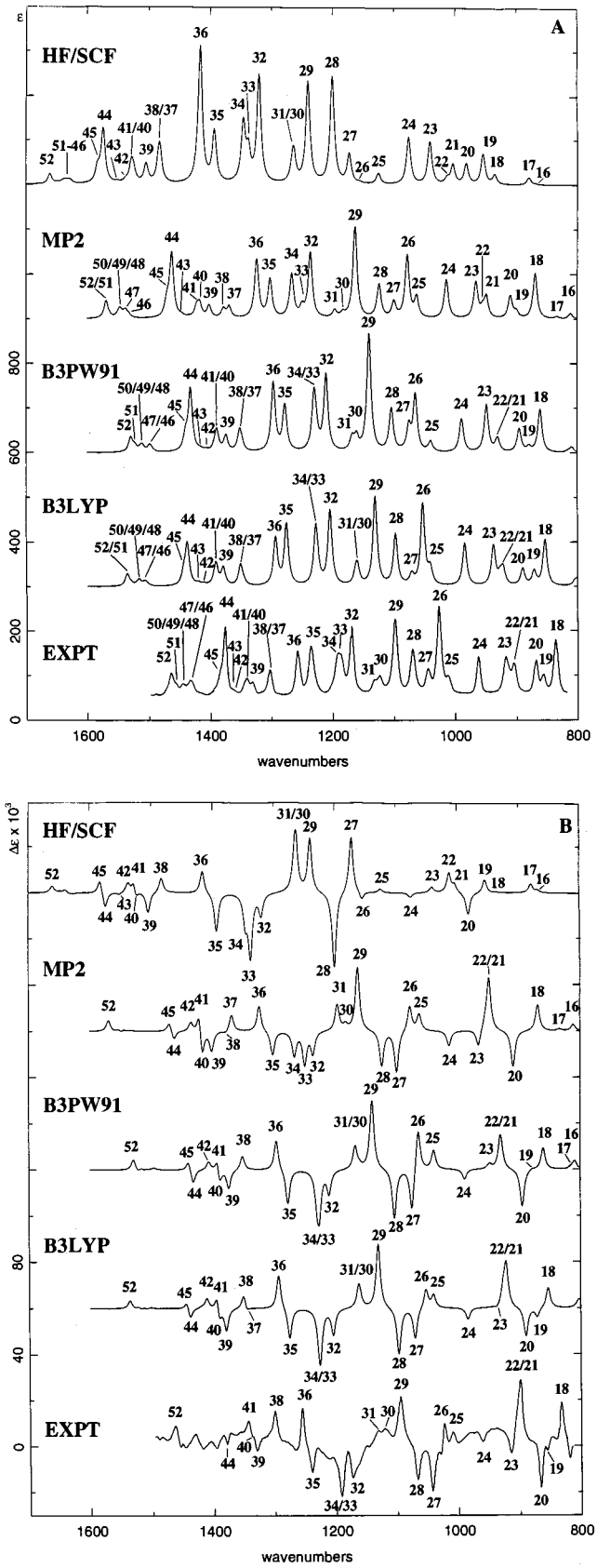

Figure 5. (A) Unpolarized absorption and (B) VCD spectra of **5**. Fundamentals are numbered. Calculated spectra use Lorentzian band shapes ($\gamma = 4.0$ cm^{-1}).

B3LYP and B3PW91 calculations yield very similar spectra, excepting for modes 26−29, where the predicted frequency and intensity patterns are quite different. The B3LYP calculation is in much better agreement with experiment and our assignment is based on this calculation.

***exo*-7-Methyl-d$_3$-6,8-dioxabicyclo[3.2.1]octane (7).** Modes 1−45 are all straightforwardly assignable, with the exception

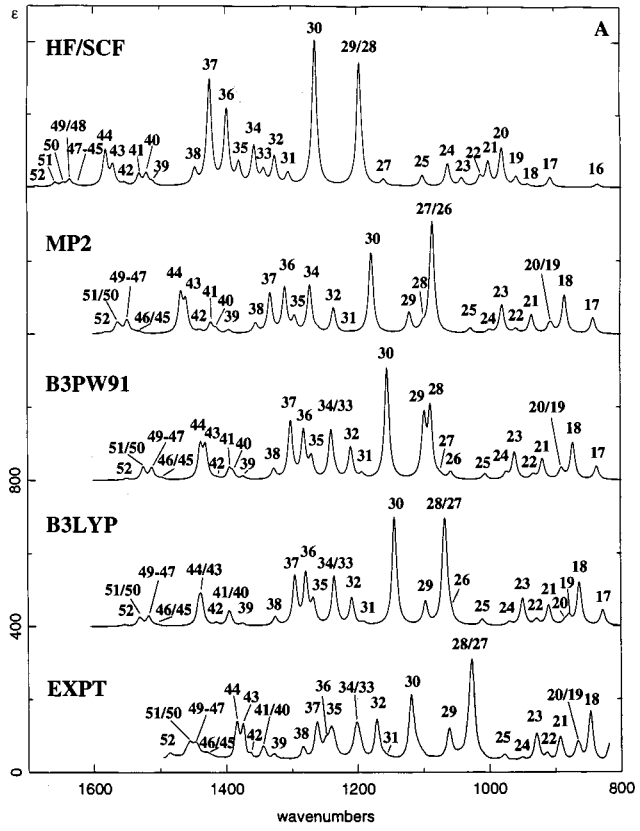

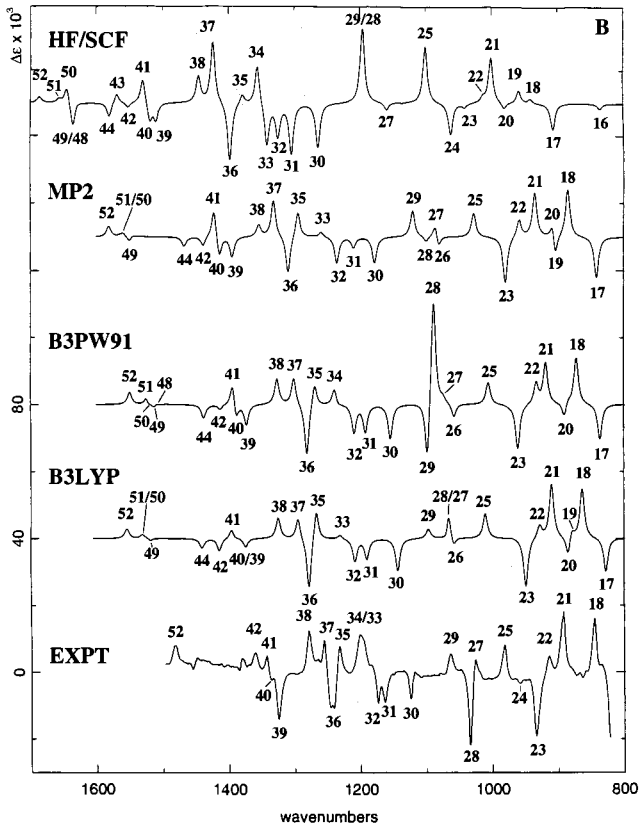

Figure 6. (A) Unpolarized absorption and (B) VCD spectra of **6**. Fundamentals are numbered. Calculated spectra use Lorentzian band shapes ($\gamma = 4.0$ cm^{-1}).

of mode 17. Modes 11 and 13 are barely detectable in the IR spectrum but are more prominent in the Raman spectrum.[13] Mode 17 may be unresolved from mode 18 or may be too weak to be observable.

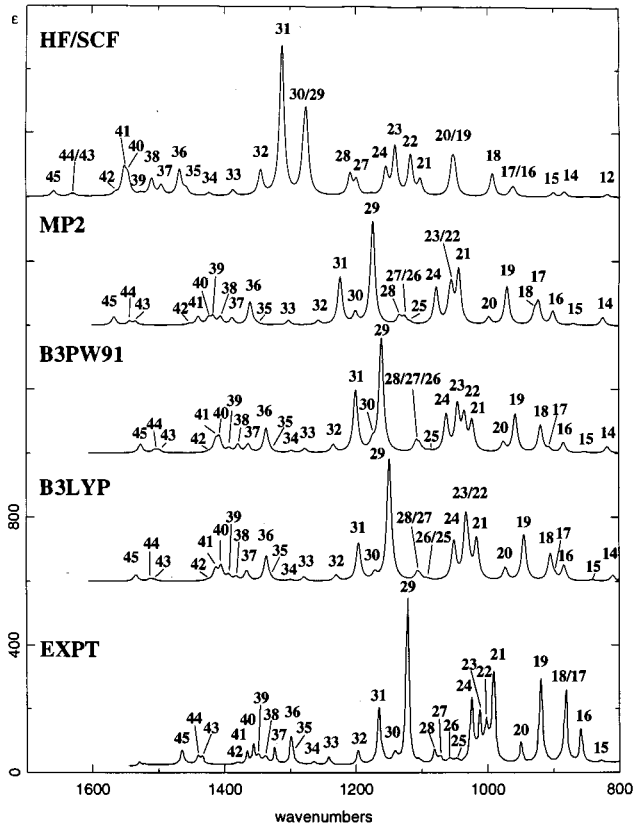

Figure 7. Unpolarized absorption spectra of **7**. Fundamentals are numbered. Calculated spectra use Lorentzian band shapes ($\gamma = 4.0$ cm^{-1}).

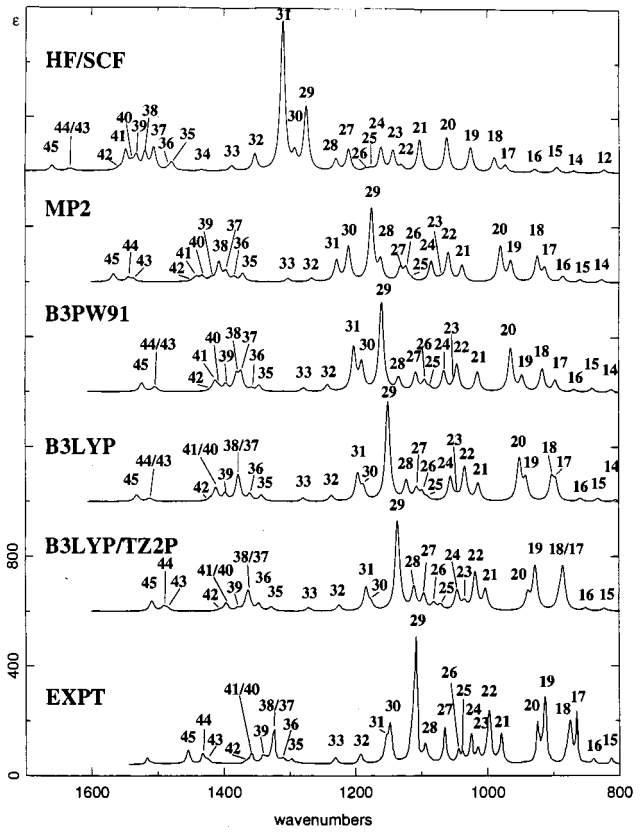

Figure 8. Unpolarized absorption spectra of **8**. Fundamentals are numbered. Calculated spectra use Lorentzian band shapes ($\gamma = 4.0$ cm^{-1}).

B3PW91 and B3LYP calculations yield very similar spectra and identical assignments.

TABLE 2: *exo*-7-Methyl-6,8-dioxabicyclo[3.2.1]octane (2): Experimental and Calculated Frequencies, Dipole Strengths, and Rotational Strengths[a]

			calculations[c]											
experiment[b]			B3LYP			B3PW91			MP2			HF/SCF		
ν	D	fund.	ν	D	R	ν	D	R	ν	D	R^d	ν	D	R
1462[e]	31.3	45	1533	16.8	3.5	1526	23.9	4.1	1566	21.1	4.9	1657	12.5	4.1
1456[e]	9.1	44	1528	7.8	−2.5	1522	8.8	−2.7	1559	10.9	−2.8	1642	5.9	−1.9
1453[e]	5.0													
1445	11.4	43	1517	7.1	1.0	1512	8.6	1.3	1550	9.1	1.3	1635	4.5	0.5
1439	12.7	42	1512	6.3	0.1	1504	8.6	0.4	1543	10.0	0.2	1631	4.4	−0.1
1432	15.5	41	1505	3.9	−0.2	1498	6.3	−0.2	1534	7.8	−0.7	1627	4.0	−1.2
1381	18.3	40	1437	19.1	10.2	1434	21.3	12.6	1465	25.9	12.1	1577	17.6	10.3
1369	21.9	39	1424	9.4	0.7	1418	20.0	−3.3	1447	9.7	2.8	1552	58.5	5.8
1363	15.5	38	1413	30.2	−14.4	1412	26.0	−13.4	1439	21.5	−18.2	1551	11.0	12.4
1354[e]	22.4	37	1406	31.8	17.8	1408	31.1	19.2	1425	13.6	13.1	1545	39.6	−21.8
1347[e]	15.0	36	1393	14.3	−5.7	1391	11.3	−12.0	1416	25.3	−6.4	1524	7.0	−6.9
1343[e]	16.3													
1335	11.6	35	1381	9.7	2.0	1378	20.0	8.2	1405	18.2	5.5	1509	36.5	14.0
1322[e]	13.8													
1318[e]	12.2	34	1366	30.5	15.9	1364	26.6	17.7	1388	22.3	20.3	1496	27.2	11.8
1315[e]	8.5													
1298	33.1	33	1340	53.3	7.6	1339	50.0	2.1	1366	45.8	0.8	1470	54.3	2.2
1288[e]	<3.0	32	1330	4.2	−4.4	1332	3.0	−2.7	1354	2.6	−3.8	1460	9.9	−3.3
1266	0.3	31	1303	1.0	−5.4	1300	1.3	−5.5	1323	2.0	−1.2	1427	2.2	−6.4
1241	12.3	30	1279	13.8	−7.9	1278	14.4	−10.8	1302	13.6	−9.0	1387	16.9	−10.4
1219														
1198	17.3	29	1231	12.1	4.6	1235	16.0	7.2	1259	7.3	0.2	1346	50.4	16.5
1163	133.0	28	1196	111.9	−28.6	1199	186.9	−42.1	1220	147.4	−38.8	1314	400.0	−83.9
1122	308.0	27	1151	274.7	−46.9	1160	341.8	−21.2	1175	80.8	−15.5	1277	279.5	−7.4
1114[e]	77.9	26	1145	101.9	34.5	1148	11.2	27.0	1173	234.5	25.1	1241	13.7	31.7
1086	16.2	25	1113	15.8	−11.1	1116	14.6	−22.3	1140	12.6	−14.3	1220	59.9	24.1
1074	26.7	24	1091	41.9	44.1	1105	44.8	51.6	1129	40.1	39.9	1205	65.4	73.5
1050[e]	26.7	23	1072	30.6	10.2	1080	38.6	4.7	1100	40.8	9.2	1165	75.7	7.2
1043	118.0	22	1069	101.5	1.5	1069	120.3	11.7	1091	78.3	13.2	1159	51.9	−26.9
1016	286.0	21	1039	243.3	−69.5	1051	208.6	−56.0	1064	201.3	−55.1	1138	147.3	−34.6
990	91.4	20	1004	109.4	9.6	1010	86.9	0.4	1034	77.5	−10.1	1086	140.5	48.2
939	319.0	19	961	232.9	111.1	978	203.7	100.5	989	212.8	107.0	1076	139.4	11.8
927	46.0	18	942	22.8	17.8	952	20.7	23.2	975	26.9	18.6	1030	17.7	24.9
885	163.0	17	904	82.7	−19.2	918	89.3	−17.2	922	89.3	−15.6	989	79.7	−4.4
870	34.7	16	890	39.4	11.3	891	21.9	5.0	908	19.7	11.3	966	36.2	−2.9
843	131.0	15	859	85.7	−23.6	872	80.0	−27.9	878	89.2	−25.5	941	45.2	−21.2
832	<8.0	14	843	3.3	−1.3	854	3.4	0.2	872	5.3	−2.4	909	9.7	−1.7
811*	3.9	13	822	1.8	−0.4	829	3.5	−1.0	849	7.8	−1.9	880	1.1	0.0
764*	41.2	12	779	2.9	−0.3	784	1.0	0.1	787	4.0	−1.4	848	3.4	0.2
732*	11.2	11	746	6.2	9.8	749	8.0	9.1	759	9.0	10.3	812	12.8	7.0
614	40.3	10	622	31.1	−4.4	621	30.0	−2.4	630	31.2	−4.6	676	53.8	−3.6
586	22.7	9	591	17.9	−4.0	592	16.9	−4.7	598	26.1	−3.1	640	18.2	−5.0
447	68.0	8	451	60.6	−2.2	451	59.7	−2.2	458	66.5	−2.1	483	56.0	−2.6
424	50.0	7	423	40.8	2.8	422	39.9	3.6	424	44.6	4.5	459	54.3	6.0
386		6	389	4.7	1.8	388	5.1	1.9	397	7.4	1.3	415	7.8	1.9
292		5	294	16.7	−10.9	294	16.4	−11.6	306	19.8	−15.1	315	20.8	−15.1
275		4	274	14.1	0.3	273	14.6	0.3	282	11.7	0.9	292	15.0	−0.3
251		3	252	1.5	1.1	253	1.7	1.2	272	2.9	2.0	271	0.8	3.0
228		2	230	13.1	4.7	230	14.8	5.2	242	19.6	5.8	244	11.2	4.8
188														
124		1	125	38.1	0.8	124	38.0	0.7	129	45.7	0.8	135	45.9	0.9

[a] ν in cm^{-1}; D in 10^{-40} esu^2 cm^2; R in 10^{-44} esu^2 cm^2. Rotational strengths are for the (1*R*,5*S*,7*R*) enantiomer. [b] From IR spectra of CCl_4 or CS_2 solutions of racemic **2** above 400 cm^{-1} and IR spectra of gaseous **2** below 400 cm^{-1}. Parameters from CS_2 solutions are asterisked. [c] All calculations use the 6-31G* basis set. [d] Calculated using semi-MP2 distributed origin gauge AATs. [e] From deconvolved spectra.

***endo*-7-Methyl-d_3-6,8-dioxabicyclo[3.2.1]octane (8).** Modes 3−33, 35, 36, 39, and 42−45 are straightforwardly assignable. Mode 4 is only detected in the Raman spectrum.[13] Modes 13 and 34 are very weak but are also detectable in the Raman spectrum.[13] Modes 1/2, 37/38, and 40/41 are not resolved.

B3LYP and B3PW91 calculations yield overall very similar spectra and identical assignments.

We turn now to the VCD spectra of **2**−**6**. The VCD spectra of CCl_4 solutions of **2**−**6** over the range 800−1500 cm^{-1} are shown in Figures 2−6. Rotational strengths predicted using DFT, 6-31G*, and the functionals B3LYP and B3PW91 are given in Tables 2−6. VCD spectra predicted thence are shown in Figures 2−6.

For each molecule, the B3LYP and B3PW91 VCD spectra are overall qualitatively very similar. Both functionals predict spectra in good overall agreement with experiment and confirm the assignment of fundamentals arrived at from the absorption spectra. In some cases, comparison of predicted and experimental VCD spectra enable assignments to be made in greater detail than was possible using absorption spectra alone.

TABLE 3: *endo*-7-Methyl-6,8-dioxabicyclo[3.2.1]octane (3): Experimental and Calculated Frequencies, Dipole Strengths, and Rotational Strengths[a]

experiment[b]			calculations[c]														
			B3LYP						B3PW91			MP2			HF/SCF		
ν	D	fund.	ν		D		R		ν	D	R	ν	D	R^d	ν	D	R
1466	39.2	45	1535	*1511*	20.9	*34.3*	6.5	*7.8*	1528	24.1	8.7	1570	30.6	8.5	1660	17.9	5.2
1457[e]	5.1	44	1528	*1503*	4.4	*3.3*	−2.0	*−2.1*	1521	9.9	−3.8	1562	1.4	−0.7	1647	1.0	0.3
		43	1520	*1496*	2.7	*5.6*	0.8	*1.2*	1515	2.6	0.6	1552	1.4	0.7	1639	3.7	0.8
1434	27.3	42	1508	*1485*	3.6	*8.4*	0.4	*0.9*	1501	5.3	1.7	1539	12.7	−0.4	1628	4.0	−0.6
1432[e]	7.7	41	1506	*1483*	8.6	*17.0*	0.3	*−0.4*	1499	12.4	0.8	1535	11.6	1.4	1627	4.7	−0.5
1384	49.0	40	1441	*1418*	38.1	*43.4*	−0.8	*1.8*	1437	46.9	0.5	1469	43.8	−0.2	1579	29.2	1.3
1370[e]	6.7	39	1422	*1407*	1.6	*2.6*	1.5	*−2.6*	1419	4.7	−3.7	1448	1.5	0.2	1553	9.2	−6.9
1364[e]	13.4	38	1412	*1395*	16.2	*18.0*	−9.3	*−15.1*	1411	17.9	−12.5	1440	9.8	−9.3	1547	58.5	−5.1
1359[e]	16.4	37	1409	*1394*	21.3	*3.0*	4.5	*5.9*	1406	17.3	10.0	1430	14.6	0.9	1539	17.3	4.2
1347	17.9	36	1398	*1379*	26.0	*10.2*	9.7	*8.9*	1396	23.0	10.2	1419	12.5	1.6	1531	36.0	15.2
1336[e]	16.4	35	1379	*1365*	34.5	*19.5*	−9.0	*−5.5*	1381	34.7	−5.5	1407	50.7	10.6	1519	33.9	0.8
1334[e]	24.0																
1330[e]	42.7	34	1376	*1363*	38.2	*43.1*	0.3	*−3.4*	1373	49.0	−5.3	1397	27.0	−9.0	1505	57.7	−10.3
1317	12.5	33	1360	*1347*	19.4	*22.2*	−1.6	*8.1*	1357	7.4	1.2	1384	8.4	0.2	1483	5.0	0.7
1305	12.8	32	1343	*1328*	21.3	*13.7*	2.2	*−0.3*	1347	21.6	2.0	1373	28.9	3.1	1479	23.9	1.4
1289	0.2																
1265	0.3	31	1311	*1301*	0.4	*0.1*	−1.4	*1.2*	1310	0.4	−1.1	1329	0.2	0.9	1435	2.8	−3.7
1240	20.3	30	1278	*1270*	12.6	*13.2*	−7.8	*−13.7*	1278	14.1	−11.6	1301	11.9	−8.2	1387	16.1	−10.5
1204	31.6	29	1237	*1226*	25.1	*25.2*	0.7	*2.5*	1242	30.9	2.8	1267	15.2	−1.3	1354	60.7	7.8
1190[e]																	
1163	137.0	28	1196	*1186*	128.9	*85.4*	−12.3	*−8.5*	1199	210.2	−17.9	1220	152.6	−19.7	1313	418.4	−56.3
1139	21.7	27	1169	*1160*	39.9	*40.0*	24.0	*24.1*	1171	28.9	26.1	1196	4.7	19.9	1277	157.3	14.2
1132[e]	1.2																
		26	1141	*1130*	0.5	*13.9*	5.0	*−25.7*	1149	365.7	−22.3	1174	42.0	44.5	1256	174.3	−33.2
1113	435.0																
		25	1135	*1120*	401.1	*363.0*	−38.3	*2.4*	1145	2.4	−8.6	1167	308.3	−47.7	1242	16.9	23.6
1098[e]	1.6																
1077	131.0	24	1105	*1093*	77.1	*105.0*	4.8	*−3.4*	1112	78.9	1.6	1135	75.6	0.1	1215	97.3	31.1
1055	10.7	23	1080	*1070*	6.3	*2.3*	−4.9	*−10.0*	1084	14.0	−4.5	1104	15.5	−5.5	1172	46.6	−19.6
1041	19.3	22	1063	*1055*	7.7	*12.2*	−4.3	*−6.6*	1066	12.0	−8.5	1089	13.7	−10.3	1166	67.1	13.2
1024	275.0	21	1048	*1035*	187.8	*228.2*	−27.4	*−46.8*	1060	155.6	−6.7	1073	154.6	−19.9	1141	33.8	4.5
979[e]	16.2																
971	70.8	20	985	*979*	88.0	*74.9*	−4.3	*−6.5*	990	83.0	−6.4	1013	72.0	−0.7	1076	235.8	43.3
931	256.0	19	953	*934*	259.3	*138.8*	100.2	*105.9*	970	245.6	82.3	982	213.5	84.0	1065	94.7	−15.5
921	167.0	18	939	*927*	60.3	*201.3*	−24.8	*−25.7*	946	45.3	−19.9	971	70.9	−30.7	1025	23.3	7.8
884	164.0	17	902	*891*	86.1	*76.4*	−17.5	*−32.1*	915	94.4	−12.7	923	89.3	−19.5	989	78.9	−0.5
874	41.9	16	893	*885*	29.4	*71.7*	6.8	*11.7*	894	10.6	2.9	910	18.7	10.0	969	28.7	2.2
843[e]	6.0																
836[e]	129.0	15	853	*840*	82.6	*91.7*	18.1	*19.9*	864	80.1	18.8	875	63.3	11.3	936	50.5	9.3
831[e]	18.3	14	843	*833*	3.0	*2.6*	−1.9	*−2.4*	854	2.5	−1.5	868	30.7	7.9	908	13.1	1.2
793*	6.1	13	804	*795*	3.1	*3.4*	5.1	*8.0*	812	4.3	3.7	832	7.8	8.2	865	2.6	1.2
758*	16.7	12	772	*767*	9.5	*13.5*	8.7	*13.7*	775	6.4	9.7	778	7.2	7.3	840	8.8	8.3
719*	5.8	11	721	*717*	2.7	*1.8*	−3.0	*−2.0*	725	4.8	−4.4	744	4.0	−5.0	782	8.9	−7.8
617	39.7	10	624	*623*	27.5	*24.7*	−5.9	*−7.3*	623	25.9	−4.8	634	32.2	−4.4	680	44.4	−5.3
515	33.9	9	518	*515*	20.6	*19.9*	2.3	*2.8*	519	21.9	2.7	527	27.1	4.0	560	21.6	3.9
475	29.9	8	479	*479*	20.5	*20.7*	−8.4	*−8.1*	476	20.8	−8.1	484	20.6	−9.1	517	29.6	−10.2
436	59.4	7	442	*442*	51.9	*46.3*	4.3	*3.5*	440	51.1	4.4	446	52.2	2.7	474	43.0	3.3
		6	361	*360*	62.6	*65.8*	1.7	*6.2*	360	59.9	4.7	364	76.3	2.7	389	66.0	12.0
356																	
		5	356	*356*	3.9	*8.4*	−3.6	*−7.3*	355	7.5	−6.3	360	4.2	−3.0	382	20.7	−12.5
273		4	272	*266*	0.0	*0.4*	0.1	*1.0*	274	0.0	−0.1	293	0.5	−0.6	292	1.3	−0.3
		3	220	*216*	3.2	*2.2*	−0.8	*−1.1*	221	3.5	−0.5	231	3.4	−1.1	235	1.7	−1.0
221																	
		2	213	*200*	3.4	*2.5*	−0.1	*1.8*	213	4.7	−0.7	227	3.3	0.3	227	1.4	1.8
164		1	156	*152*	39.9	*45.6*	−1.4	*−2.2*	156	39.4	−1.6	169	47.1	−2.4	170	46.9	−2.6

[a] ν in cm^{-1}; D in 10^{-40} esu^2 cm^2; R in 10^{-44} esu^2 cm^2. Rotational strengths are for the (1*R*,5*S*,7*S*) enantiomer. [b] From IR spectra of CCl_4 or CS_2 solutions of racemic **3** above 400 cm^{-1} and IR spectra of gaseous **3** below 400 cm^{-1}. Parameters from CS_2 solutions are asterisked. [c] All calculations use the 6-31G* basis set, except numbers in italic type, which have been obtained using the TZ2P basis set. [d] Calculated using semi-MP2 Distributed Origin gauge AATs. [e] From deconvolved spectra.

***exo*-7-Methyl-6,8-dioxabicyclo[3.2.1]octane (2).** The VCD of fundamentals 15, 16, 18−21, 24−31, 34, 36−38, and 40 is clearly observed. Signs and magnitudes are in good overall agreement with predictions for both functionals. Negative VCD at ∼840 cm^{-1} may originate from mode 14. B3LYP and B3PW91 predict weak VCD of negative and positive sign, respectively. The VCD corresponding to mode 17 is bisignate and in poor agreement with calculation; both functionals predict negative VCD. B3LYP and B3PW91 both predict positive VCD for modes 22 and 23; however, predicted relative magnitudes are very different. Positive VCD is observed but the two modes are not resolved and their relative intensities cannot be compared to predictions. Only very weak absorption was observed for mode 31; the observation of VCD confirms

TABLE 4: *exo*-5,7-Dimethyl-6,8-dioxabicyclo[3.2.1]octane (4): Experimental and Calculated Frequencies, Dipole Strengths, and Rotational Strengths[a]

experiment[b]			calculations[c]											
			B3LYP			B3PW91			MP2			HF/SCF		
ν		fund.	ν	D	R	ν	D	R	ν	D	R^d	ν	D	R
		52	1531	17.0	3.2	1524	25.6	2.5	1566	19.5	4.8	1658	10.2	3.8
1457														
		51	1528	5.5	−0.5	1522	5.6	1.3	1559	9.3	−0.3	1643	4.2	0.5
		50	1519	11.2	0.0	1514	13.2	0.0	1551	12.1	1.8	1636	8.8	−1.1
1439		49	1517	2.0	−1.3	1512	3.1	−1.3	1547	3.1	−3.9	1634	2.4	−1.5
		48	1516	5.1	0.7	1510	4.7	0.5	1546	11.4	0.7	1632	4.2	1.5
		47	1509	4.9	0.5	1501	7.6	1.0	1541	7.3	0.8	1630	0.7	−0.3
1422														
		46	1503	1.9	0.4	1495	3.0	0.2	1531	4.0	−0.4	1626	1.3	−0.5
	1384	45	1440	60.0	−6.0	1436	78.8	−11.0	1466	68.3	−8.0	1579	38.2	−6.9
1378														
	1378	44	1435	36.9	12.5	1431	58.5	17.2	1462	68.5	15.6	1574	73.3	11.6
1366		43	1422	2.9	4.7	1416	4.5	5.0	1447	6.1	5.0	1552	3.1	1.6
	1352	42	1401	1.0	2.0	1398	0.8	−1.3	1425	3.6	−10.6	1531	23.6	−1.8
1345		41	1395	36.1	6.3	1394	33.9	10.5	1423	30.9	17.2	1528	13.8	21.2
	1333	40	1384	13.1	−3.4	1379	5.9	−11.5	1405	5.9	−10.7	1513	33.7	−6.0
1326														
		39	1376	26.2	0.7	1376	34.7	3.1	1395	25.7	3.2	1508	21.1	−12.5
1293		38	1337	11.0	−4.1	1338	8.0	−5.9	1365	13.1	−4.6	1475	17.8	−10.0
1284		37	1329	36.2	−11.8	1328	34.8	−7.8	1355	18.9	−10.0	1453	41.4	−7.8
1243		36	1287	28.5	42.6	1286	87.8	67.1	1313	66.6	62.8	1409	271.7	63.1
1233		35	1274	175.7	−2.8	1279	136.9	−28.0	1303	123.7	−19.0	1393	82.0	−29.5
1192		34	1227	107.9	−38.2	1229	119.1	−43.4	1263	99.2	−31.2	1339	120.8	−56.7
1182		33	1221	58.1	−9.3	1222	64.2	−13.4	1246	43.8	−20.5	1335	68.3	4.7
1170		32	1204	148.5	−29.5	1210	128.1	−23.4	1236	113.7	−20.5	1320	173.0	−32.1
1126		31	1162	28.3	16.8	1163	44.6	12.7	1187	26.5	14.4	1268	56.3	1.6
1099		30	1136	103.9	−18.4	1140	130.4	−20.6	1162	87.0	−8.1	1241	110.5	−7.2
1070		29	1098	60.5	−1.0	1106	72.4	80.0	1131	52.0	50.0	1212	125.3	144.2
1065		28	1091	43.3	41.7	1098	67.7	−24.7	1119	55.3	−8.6	1194	36.0	−23.6
1054		27	1077	79.9	31.1	1085	77.8	23.4	1106	70.9	22.4	1170	184.1	−28.2
1018		26	1047	192.8	−57.8	1056	283.7	−64.1	1069	158.1	−52.4	1149	149.4	−40.5
1009		25	1038	152.8	−15.3	1039	17.8	8.5	1061	75.9	−3.3	1127	36.5	10.5
976		24	998	135.0	21.0	1006	88.0	21.5	1029	158.3	8.8	1086	63.8	33.2
924		23	946	90.5	65.5	957	93.7	67.1	972	84.8	48.3	1043	74.3	40.5
913		22	931	28.7	25.1	937	27.9	29.0	960	25.5	19.6	1018	36.2	25.4
905		21	926	26.0	27.5	933	9.7	9.7	953	28.2	45.7	1007	27.0	5.8
869		20	895	35.3	−35.0	900	42.5	−41.7	913	49.3	−41.4	979	47.7	−32.7
849		19	871	16.5	−0.4	878	7.5	6.5	897	11.1	7.7	957	108.4	−3.9
834		18	856	175.2	−6.5	866	157.4	−11.9	872	149.6	−4.9	937	16.0	−7.9
		17	823	5.2	−1.2	830	1.9	−0.5	851	7.0	−2.0	887	6.5	0.4
		16	801	11.2	1.7	810	9.2	1.7	812	7.8	−3.0	877	8.7	0.9
		15	747	2.5	4.8	751	2.5	5.5	762	2.4	8.1	815	3.6	4.9
		14	639	6.2	−2.9	643	7.6	−2.8	651	11.7	−7.3	690	12.1	−1.4
		13	620	33.1	−11.3	619	30.0	−11.5	631	34.2	−9.3	676	49.6	−14.3
		12	562	19.4	2.5	564	18.9	2.9	573	23.3	3.9	607	21.9	4.4
		11	470	45.1	−5.3	470	43.7	−5.0	479	54.0	−5.6	505	50.3	−5.7
		10	436	27.1	5.4	435	27.4	5.9	439	29.8	6.9	473	32.4	7.9
		9	402	10.2	7.0	402	11.0	7.8	412	10.5	7.6	431	7.3	7.0
		8	352	43.9	−9.3	353	43.8	−10.4	362	49.9	−13.0	382	49.1	−11.0
		7	317	8.2	−0.4	316	8.2	−0.6	325	6.5	−0.6	339	7.5	−0.3
		6	276	23.7	−2.8	277	24.4	−2.7	291	22.2	−1.3	296	23.0	−4.8
		5	254	1.5	0.5	255	1.7	0.2	273	2.0	1.4	272	1.1	−0.9
		4	241	7.5	3.2	241	6.6	3.8	249	1.9	2.1	258	7.5	4.9
		3	225	12.5	−0.2	225	14.0	−0.7	241	20.5	−0.5	245	9.4	−0.4
		2	206	6.5	0.3	208	8.0	0.8	229	13.0	2.1	231	7.9	2.1
		1	115	31.4	−0.2	114	31.6	−0.5	118	37.2	−1.1	125	37.3	−0.8

[a] ν in cm^{-1}; D in 10^{-40} esu^2 cm^2; R in 10^{-44} esu^2 cm^2. Rotational strengths are for the (1*R*,5*S*,7*R*) enantiomer. [b] Peak frequencies from IR spectra of CCl_4 solutions of racemic **4**. Frequencies in italic type are from the VCD spectrum. [c] All calculations use the 6-31G* basis set. [d] Calculated using semi-MP2 distributed origin gauge AATs.

its assignment. Both functionals predict negative and positive VCD for modes 32 and 33, respectively. The negative VCD of mode 32 is clearly observed, while the positive VCD of mode 33 is not. Weak positive VCD is predicted for mode 35 by both functionals. For mode 39, B3LYP and B3PW91 predict weak positive and negative VCD, respectively. Experimentally, VCD is not clearly detectable for either mode 35 or 39. Very weak VCD is predicted for modes 41−45. Consistently, VCD is not clearly observable for these modes.

***endo*-7-Methyl-6,8-dioxabicyclo[3.2.1]octane (3).** The VCD of fundamentals 17−24 and 27−31 is clearly observed. Signs and magnitudes are in moderate agreement with predictions for both functionals. For modes 17−20, the spectra predicted by the two functionals are very similar; the experimental VCD is

TABLE 5: *endo*-5,7-Dimethyl-6,8-dioxabicyclo[3.2.1]octane (5): Experimental and Calculated Frequencies, Dipole Strengths, and Rotational Strengths[a]

		calculations[c]											
experiment[b]		B3LYP			B3PW91			MP2			HF/SCF		
ν	fund.	ν	D	R	ν	D	R	ν	D	R^d	ν	D	R
1464	52	1535	20.6	6.4	1529	24.3	8.7	1569	29.0	8.6	1660	15.3	4.9
1456	51	1529	3.5	−0.5	1522	8.7	−2.0	1562	1.4	−0.5	1648	1.8	0.7
	50	1520	0.9	1.2	1515	0.9	1.5	1551	1.1	1.4	1639	4.4	2.3
1445	49	1517	7.0	−1.7	1512	8.5	−2.0	1548	7.4	−2.7	1634	3.6	−1.1
	48	1515	4.5	0.8	1509	4.6	1.2	1546	9.4	2.1	1631	2.0	0.1
	47	1506	7.6	−0.7	1498	10.6	0.3	1538	12.3	0.3	1627	3.7	−0.2
1433													
	46	1503	2.1	1.1	1495	3.5	1.2	1532	5.4	0.6	1626	1.5	−0.9
1384	45	1444	19.9	6.3	1440	25.9	8.1	1470	26.3	7.6	1583	23.3	10.6
1376	44	1437	75.0	−9.5	1432	112.7	−12.7	1462	113.7	−7.9	1574	88.9	−12.7
1365	43	1419	4.6	1.2	1416	3.0	0.0	1446	3.5	−0.1	1551	2.3	−1.8
1360	42	1411	3.2	8.7	1407	2.4	7.3	1435	1.6	7.7	1537	4.5	7.6
1344	41	1394	4.9	16.4	1392	3.8	13.6	1421	18.6	19.9	1528	34.1	9.4
1341													
	40	1391	39.3	−15.4	1389	40.1	−15.6	1417	24.2	−25.1	1524	15.7	−6.5
1332	39	1379	33.2	−20.1	1374	29.4	−17.3	1401	22.5	−17.8	1504	32.3	−17.1
	38	1351	40.5	12.8	1351	40.6	13.0	1378	16.8	−2.5	1483	49.2	12.5
1303													
	37	1345	5.6	−4.4	1347	9.1	−0.2	1369	21.3	15.1	1481	26.5	−0.1
1258	36	1293	94.3	33.1	1296	137.6	29.4	1323	115.4	24.3	1416	251.5	20.2
1236	35	1275	124.9	−30.3	1277	93.7	−34.4	1301	77.0	−23.4	1393	94.2	−35.3
1192	34	1227	99.4	−18.4	1229	114.0	−28.7	1266	88.9	−24.3	1346	113.0	−26.6
1187	33	1225	34.2	−42.7	1226	26.9	−39.1	1249	20.2	−32.8	1337	56.1	−58.5
1169	32	1204	161.4	−26.8	1210	163.3	−24.1	1236	137.7	−22.7	1320	210.7	−20.5
1132	31	1162	23.0	24.4	1167	28.7	24.3	1196	15.8	27.5	1265	33.3	26.4
1124	30	1159	37.1	2.7	1160	29.9	3.3	1182	10.1	5.8	1263	44.7	39.9
1098	29	1130	203.4	71.5	1140	269.5	76.7	1162	205.2	68.7	1240	214.2	54.3
1070	28	1097	120.4	−53.0	1103	100.9	−56.3	1123	77.0	−39.4	1200	231.6	−80.3
1044	27	1070	24.8	−35.8	1075	57.9	−51.4	1099	36.9	−47.7	1172	64.5	60.2
1026	26	1052	200.8	22.6	1064	136.6	50.5	1077	149.7	29.3	1155	3.2	−8.9
1012	25	1040	39.1	15.3	1039	25.4	22.8	1062	49.1	19.5	1124	24.6	4.3
962	24	984	112.8	−14.5	989	87.3	−12.8	1013	100.0	−18.5	1075	114.0	−5.2
918	23	937	109.8	−3.3	948	130.0	6.7	966	96.6	−22.6	1040	106.3	6.6
	22	927	24.4	21.7	931	30.5	35.0	955	19.2	7.3	1012	14.3	24.1
905													
	21	922	45.1	56.1	929	9.0	14.0	949	56.9	70.2	1003	49.8	9.5
868	20	890	49.7	−40.2	895	67.6	−53.1	909	64.3	−49.9	981	53.5	−28.4
857	19	871	42.5	−12.8	879	14.7	2.3	900	18.2	0.0	954	82.0	17.9
836	18	853	140.6	30.2	861	129.2	31.4	869	135.8	38.3	935	25.8	0.9
	17	805	10.1	4.7	815	5.0	3.1	834	6.7	3.0	880	21.9	12.3
	16	801	20.8	11.1	809	17.0	12.8	811	17.9	10.3	869	1.9	3.2
	15	723	3.6	−0.5	727	4.0	−1.6	744	3.0	−2.4	783	6.4	−5.8
	14	632	9.9	1.3	635	8.3	2.8	643	12.3	3.4	688	19.8	1.1
	13	606	38.1	−14.9	606	36.6	−15.9	619	41.0	−16.6	656	50.2	−14.6
	12	526	26.7	0.7	527	27.7	0.6	536	34.1	1.0	570	29.8	2.0
	11	470	28.0	−3.9	470	28.3	−3.9	477	34.9	−4.4	508	36.1	−3.7
	10	449	30.4	1.4	447	30.2	1.9	455	29.2	2.0	482	22.6	0.7
	9	423	17.6	−1.5	422	18.5	−1.2	428	20.7	−1.1	457	20.4	−2.3
	8	388	20.9	6.9	387	21.0	7.2	394	24.9	7.2	418	27.1	7.6
	7	281	22.2	−1.1	281	19.8	0.0	301	8.6	1.1	304	17.3	1.0
	6	275	11.0	−3.4	275	14.0	−4.5	283	23.3	−6.7	295	17.0	−5.7
	5	258	15.1	2.8	259	15.3	3.0	271	14.5	5.1	279	15.4	4.2
	4	220	2.0	−0.5	220	2.3	−0.5	234	6.0	3.3	236	1.4	0.0
	3	217	1.8	0.0	215	2.9	−0.1	231	5.8	−6.8	233	4.6	−1.3
	2	206	5.9	−0.4	207	6.7	−0.4	226	3.6	2.1	227	1.3	1.4
	1	144	44.0	−3.6	145	44.3	−4.1	157	49.6	−4.9	160	48.0	−4.6

[a] ν in cm^{-1}; D in 10^{-40} esu^2 cm^2; R in 10^{-44} esu^2 cm^2. Rotational strengths are for the (1*R*,5*S*,7*S*) enantiomer. [b] From IR spectra of CCl_4 solutions of racemic **5**. Frequencies in italic type are from the VCD spectrum. [c] All calculations use the 6-31G* basis set. [d] Calculated using semi-MP2 distributed origin gauge AATs.

considerably larger than predicted for modes 17, 18, and 20 but smaller for mode 19. While both functionals predict negative VCD for modes 21−23, predicted relative intensities are significantly different. The experimental VCD is in better qualitative agreement with the B3LYP calculation. Both functionals predict positive VCD for mode 24, whereas the observed VCD is negative. For modes 27−31, the two functionals yield very similar predicted spectra which are in good agreement with experiment. Mode 31 is very weak in the absorption spectrum; observation of its VCD confirms its assignment. The VCD of modes 25 and 26 are not resolved. Both functionals predict predominantly negative VCD as observed.

Analysis of the VCD above 1300 cm^{-1} is complicated by the greater density of transitions, the weak VCD intensity of a large fraction of modes 32−45 and greater noise in the

TABLE 6: 1,5-Dimethyl-6,8-dioxabicyclo[3.2.1]octane (6): Experimental and Calculated Frequencies, Dipole Strengths, and Rotational Strengths[a]

			calculations[c]											
experiment[b]			B3LYP			B3PW91			MP2			HF/SCF		
ν		fund.	ν	D	R	ν	D	R	ν	D	R^d	ν	D	R
1486		52	1554	3.3	5.3	1550	3.9	6.8	1581	3.1	5.8	1686	2.0	3.1
		51	1531	14.4	2.0	1524	23.4	4.5	1563	18.4	0.8	1656	7.6	2.0
1455														
		50	1528	5.6	0.4	1522	3.4	−2.0	1559	8.8	1.7	1644	6.2	8.8
		49	1517	2.0	−3.1	1512	2.2	−2.9	1549	12.4	−4.4	1635	5.5	−8.2
1447		48	1517	17.7	1.6	1511	21.4	1.2	1548	10.5	1.3	1634	7.7	−5.9
		47	1515	0.9	0.4	1509	1.3	0.6	1546	5.7	1.4	1631	0.2	0.7
1427		46	1508	1.3	−0.2	1501	2.1	−0.2	1538	3.1	0.2	1628	0.2	1.3
1422		45	1503	1.9	0.3	1495	3.1	0.4	1530	4.2	0.2	1625	1.9	−0.1
1384		44	1441	40.2	−5.3	1438	70.0	−8.0	1467	79.5	−5.4	1580	70.0	−7.9
1375		43	1437	51.7	−0.7	1430	67.5	−0.3	1459	62.5	−0.1	1569	38.4	5.5
1364		42	1414	5.7	−7.4	1413	2.3	−3.0	1438	5.6	−5.5	1552	5.4	−2.8
	1343	41	1395	24.2	6.7	1394	23.5	14.2	1422	22.8	17.5	1529	23.5	14.3
1344														
	1336	40	1393	12.6	−1.6	1388	13.4	−10.2	1413	9.9	−13.1	1518	24.8	−10.7
1328		39	1375	5.6	−5.4	1373	7.1	−12.8	1394	8.1	−12.4	1509	7.6	−9.9
1283		38	1325	20.7	13.4	1326	23.9	16.6	1354	22.2	7.3	1445	33.8	15.9
1262		37	1295	117.2	13.9	1301	139.8	17.8	1331	93.8	23.5	1423	238.9	37.5
1248		36	1278	123.8	−35.6	1281	115.7	−35.6	1309	107.8	−24.8	1397	172.4	−37.3
1240		35	1267	54.8	20.8	1269	49.2	15.5	1294	34.4	17.1	1379	47.0	6.2
		34	1235	122.3	0.0	1239	122.1	11.1	1271	118.0	0.4	1356	89.5	26.0
1201														
		33	1231	7.4	2.7	1233	10.1	−1.5	1259	6.1	3.4	1341	32.2	−27.9
1171		32	1208	71.7	−16.1	1209	82.6	−19.9	1235	64.3	−18.2	1325	67.7	−21.4
1161		31	1190	7.1	−14.5	1192	12.9	−19.5	1210	2.0	−7.4	1304	28.9	−33.5
1119		30	1143	301.3	−24.3	1154	304.0	−25.5	1178	218.3	−19.0	1264	371.3	−30.8
1061		29	1096	65.7	7.2	1098	169.7	−50.0	1120	57.0	19.9	1196	290.3	33.2
		28	1069	106.9	−8.2	1088	195.1	87.2	1099	17.3	−4.4	1195	42.5	21.2
1026		27	1066	241.1	23.5	1074	7.1	4.1	1085	320.0	11.1	1159	17.0	−5.8
		26	1058	15.0	−8.0	1057	20.7	−11.0	1080	12.6	−10.0	1135	1.1	−0.6
978		25	1010	19.5	21.0	1005	17.8	19.1	1027	16.6	20.1	1100	31.8	44.6
950		24	969	11.7	0.9	974	19.2	−0.9	998	10.3	−0.2	1062	67.8	−26.5
929		23	949	92.1	−44.6	961	90.0	−40.8	979	92.4	−41.1	1040	24.6	−3.6
913		22	928	19.2	11.9	933	15.5	19.3	958	13.9	15.7	1013	29.3	4.4
893		21	910	70.7	51.2	919	70.6	38.8	935	62.2	40.0	1001	75.6	39.5
		20	885	13.3	−18.6	890	35.4	−14.4	908	25.5	20.0	980	123.3	−5.7
866														
		19	879	30.8	8.3	885	4.9	4.3	904	19.0	−26.4	958	32.0	11.7
847		18	864	159.1	49.9	872	133.9	46.9	885	136.5	46.6	941	6.9	4.0
		17	828	59.9	−35.0	836	50.0	−36.4	842	60.5	−42.0	907	33.6	−25.7
		16	764	8.1	−2.9	771	9.4	−3.3	780	5.3	−0.8	835	12.4	−5.7
		15	640	7.5	5.4	644	8.1	5.3	651	12.7	6.5	693	13.7	8.4
		14	615	38.8	−10.8	614	36.2	−10.0	627	34.5	−8.2	667	57.2	−14.5
		13	594	12.5	−2.2	599	13.8	−2.4	607	21.2	−4.9	637	11.1	3.6
		12	497	5.1	5.8	495	5.1	6.6	501	6.2	8.0	538	5.8	7.9
		11	481	42.7	−2.1	481	40.8	−2.4	489	47.2	−2.3	516	47.5	−3.3
		10	438	9.7	4.8	437	10.4	5.2	443	12.3	4.5	472	13.0	4.2
		9	393	4.6	0.0	392	4.6	−0.1	405	5.0	−0.7	422	5.4	0.0
		8	354	8.0	−1.6	353	7.9	−1.8	365	9.7	−2.0	381	8.6	−2.9
		7	297	33.1	0.4	296	33.5	0.1	308	31.3	−0.5	324	30.1	2.3
		6	279	26.1	−1.6	279	25.4	−0.9	288	25.9	2.0	303	31.5	−2.2
		5	262	0.8	1.5	264	0.9	1.7	276	2.6	3.0	278	0.6	0.7
		4	234	15.0	2.6	234	15.5	3.0	245	7.3	5.7	249	14.0	4.5
		3	209	4.7	−4.5	210	5.7	−4.9	232	16.5	−12.6	235	7.8	−5.1
		2	202	6.9	−0.3	203	7.7	−0.5	226	9.9	3.4	229	6.5	−3.0
		1	165	60.5	−5.0	166	61.8	−6.0	170	72.6	−7.9	180	69.8	−7.1

[a] ν in cm^{-1}; D in 10^{-40} esu^2 cm^2; R in 10^{-44} esu^2 cm^2. Rotational strengths are for the (1*R*,5*S*) enantiomer. [b] From IR spectra of CCl_4 solutions of racemic **6**. Frequencies in italic type are from the VCD spectrum. [c] All calculations use the 6-31G* basis set. [d] Calculated using semi-MP2 distributed origin gauge AATs.

experimental spectrum in this region. Positive VCD is observed for mode 33; the VCD of mode 32 is very weak. Predicted VCD is weak for both modes. B3LYP predicts positive and negative VCD for modes 32 and 33, while B3PW91 predicts positive VCD for both modes. Modes 34 and 35, which are unresolved in absorption, give rise to a bisignate VCD, negative at lower frequency. B3LYP and B3PW91 predictions are quite different: B3LYP predicts predominant negative VCD in mode 35, while B3PW91 predicts comparable negative VCD in both modes. Mode 36 exhibits positive VCD in good agreement with both calculations. Modes 37 and 38 exhibit bisignate VCD, positive at lower frequencies, in good agreement with the predictions of both functionals. VCD is not clearly observed for mode 39; B3LYP and B3PW91 predict weak positive and

TABLE 7: *exo*-7-Methyl-d_3-6,8-dioxabicyclo[3.2.1]octane (7): Experimental and Calculated Frequencies and Dipole Strengths[a]

			calculations[c]							
experiment[b]			B3LYP		B3PW91		MP2		HF/SCF	
ν	D	fund.	ν	D	ν	D	ν	D	ν	D
1461	26.1	45	1533	14.9	1526	20.5	1566	19.4	1657	11.9
1438	13.3	44	1512	5.3	1505	7.4	1543	8.8	1631	3.7
1432	11.1	43	1506	4.1	1498	6.6	1534	8.0	1627	4.2
1377	2.8	42	1425	2.3	1423	2.2	1452	3.6	1564	5.6
1363	16.1	41	1413	28.7	1412	27.5	1439	19.7	1551	57.0
1353	27.4	40	1405	35.3	1407	34.4	1423	15.6	1545	39.8
1345	14.0	39	1393	13.9	1392	10.0	1417	19.8	1526	5.3
1335	14.8	38	1382	9.9	1379	20.4	1405	19.9	1509	39.6
1321	20.6	37	1366	26.5	1363	21.8	1387	18.1	1495	23.7
1295	39.4	36	1336	67.4	1336	65.3	1360	60.8	1467	62.9
1282[d]	5.4	35	1328	1.9	1330	2.8	1350	3.3	1457	15.1
1262	3.7	34	1300	4.0	1297	5.7	1320	2.0	1422	7.7
1240	12.0	33	1278	11.8	1277	11.8	1302	12.7	1386	14.8
1196	22.5	32	1229	17.0	1234	22.4	1256	12.0	1344	64.6
1163	134.0	31	1195	112.7	1199	186.3	1223	139.6	1312	413.7
1139	23.8	30	1171	20.4	1174	24.7	1200	33.9	1279	77.8
1121	375.0	29	1148	385.7	1160	355.9	1173	319.2	1275	212.4
1103	3.0									
1079	27.7	28	1106	22.1	1107	32.9	1133	25.6	1208	62.1
1071	15.2	27	1102	14.0	1102	19.9	1125	18.6	1199	44.8
1057	14.6	26	1092	3.7	1096	2.7	1124	4.9	1183	1.1
1046	7.2	25	1088	2.4	1088	3.7	1117	6.5	1176	4.3
1025	178.0	24	1051	130.2	1062	123.7	1077	122.4	1154	81.8
1013	101.0	23	1033	188.5	1045	154.3	1057	46.2	1140	153.7
1004	102.0	22	1029	66.0	1034	116.7	1054	102.4	1117	129.1
994	243.0	21	1016	140.4	1023	103.6	1043	182.3	1102	49.6
953	39.7	20	973	46.8	975	35.4	997	26.9	1053	95.2
924	247.0	19	945	176.3	957	146.2	970	143.4	1050	80.6
		18	905	105.0	919	107.7	928	45.6	993	84.4
885	208.0									
		17	897	10.0	906	14.6	922	81.2	965	12.3
861	79.9	16	884	62.0	885	41.4	901	55.6	961	31.7
831	1.6	15	841	6.6	853	5.8	869	7.7	901	17.4
792*	48.9	14	810	26.3	818	27.7	824	36.1	884	20.5
768*	<0.1	13	783	0.3	786	2.5	794	2.0	850	2.5
739*	29.2	12	753	14.9	756	10.7	768	11.9	819	13.2
668	2.3	11	677	0.8	679	1.5	692	2.5	731	5.9
611	39.9	10	619	28.3	618	26.5	627	29.5	671	45.9
560	14.3	9	567	11.9	566	11.3	571	16.5	614	12.8
446	60.8	8	451	59.5	451	58.4	458	63.7	483	57.0
404	56.5	7	404	49.2	403	48.6	405	59.2	438	63.4
375		6	379	2.8	379	3.1	387	3.3	404	4.8
284		5	285	18.3	285	18.2	294	21.7	304	22.9
258		4	257	8.5	258	8.9	269	7.9	274	8.3
233		3	228	14.8	227	16.3	237	19.1	242	12.4
188		2	177	1.9	178	2.1	191	3.0	190	1.6
117		1	118	34.4	118	34.3	121	41.3	127	41.1

[a] ν in cm^{-1}; D in 10^{-40} esu^2 cm^2. [b] From IR spectra of CCl_4 or CS_2 solutions of racemic **7** above 400 cm^{-1} and IR spectra of gaseous **7** below 400 cm^{-1}. Parameters from CS_2 solutions are asterisked. [c] All calculations use the 6-31G* basis set. [d] From deconvolved spectra.

negative VCD, respectively. Positive VCD is observed for mode 40; very weak negative and positive VCD is predicted by B3LYP and B3PW91, respectively. Very weak VCD is predicted for modes 41−43 for both functionals; the origin of the VCD features observed in this region is unclear. Bisignate VCD for modes 44 and 45 is observed, negative at lower frequencies, in agreement with the predictions of both functionals.

***exo*-5,7-Dimethyl-6,8-dioxabicyclo[3.2.1]octane (4).** Below 1300 cm^{-1}, the VCD of fundamentals 20−32, 35, and 36 is clearly observed. Signs and magnitudes are in good overall agreement with the predictions of both functionals. B3LYP and B3PW91 calculations give identical qualitative predictions for modes 20−24, 30−32, 35, and 36, in excellent agreement with experiment. B3LYP and B3PW91 predictions differ for modes 25/26 (whose predicted absorption intensities were also very different) and for modes 27−29 (whose predicted absorption intensities did not differ greatly). The observed negative VCD of both modes 25 and 26 is in agreement with the B3LYP calculation and in disagreement with the B3PW91 calculation. In contrast, the positive-negative-positive VCD of modes 27−29 is in good agreement with the B3PW91 calculation and in disagreement with the B3LYP calculation, which predicts a positive-positive-negative sign pattern. For modes 18 and 19, predictions differ; B3PW91 and B3LYP predict opposite and identical signs, respectively. Bisignate VCD is observed in qualitative agreement with the B3PW91 calculation. Quantitatively, the observed VCD is much larger than predicted. For both modes 33 and 34, negative VCD is predicted by both functionals. The observed VCD is negative, but the two modes are not resolved. The situation is similar for modes 37 and 38, except that they are better resolved in the experimental VCD.

TABLE 8: *endo*-7-Methyl-d_3-6,8-dioxabicyclo[3.2.1]octane (8): Experimental and Calculated Frequencies and Dipole Strengths[a]

experiment[b]			calculations[c]									
			B3LYP				B3PW91		MP2		HF/SCF	
ν	D	fund.	ν		D		ν	D	ν	D	ν	D
1460	31.4	45	1531	*1508*	18.3	*28.5*	1523	24.2	1566	21.1	1659	14.1
1440[d]	17.0	44	1513	*1491*	6.7	*12.2*	1505	9.8	1544	11.6	1633	5.6
1430[d]	12.2	43	1508	*1485*	3.4	*8.7*	1501	5.4	1536	7.7	1628	3.2
1372[d]	2.7	42	1419	*1405*	5.1	*3.8*	1418	2.5	1445	3.6	1558	5.0
1367[d]	5.6	41	1412	*1396*	19.3	*22.3*	1412	28.4	1440	13.1	1548	54.3
1363[d]	21.0	40	1410	*1395*	21.3	*1.7*	1407	10.3	1432	15.6	1539	15.2
1353[d]	0.3											
1346[d]	7.7											
		39	1397	*1378*	22.1	*7.9*	1396	20.6	1418	9.2	1532	37.4
1343[d]	16.9											
1333[d]	34.7	38	1378	*1365*	42.8	*22.0*	1380	47.2	1407	57.1	1519	48.0
1330[d]	44.0	37	1376	*1362*	40.8	*48.9*	1373	53.1	1396	28.5	1505	63.4
1317[d]	11.3											
		36	1360	*1347*	21.8	*21.6*	1357	7.9	1383	12.8	1483	6.6
1315[d]	5.7											
1304	8.1	35	1342	*1327*	19.0	*13.6*	1346	19.2	1370	24.7	1478	22.1
1296	2.0											
1270	1.4	34	1310	*1300*	0.7	*0.5*	1309	0.8	1328	0.5	1433	4.1
1240	14.9	33	1279	*1271*	11.3	*11.7*	1278	12.8	1302	11.0	1387	15.3
1203	26.6	32	1236	*1224*	20.1	*20.6*	1242	23.1	1266	11.5	1352	52.0
1164[d]	55.6	31	1196	*1183*	93.5	*81.3*	1202	150.7	1228	71.1	1310	484.2
1158	109.0	30	1187	*1176*	42.0	*21.6*	1190	93.2	1210	119.1	1292	47.0
1121	370.0	29	1150	*1135*	364.5	*334.4*	1159	323.7	1175	259.2	1274	214.4
1104	50.2	28	1122	*1111*	73.3	*85.1*	1133	48.4	1161	70.5	1229	40.7
1074	90.5	27	1106	*1096*	44.5	*59.0*	1108	69.0	1131	48.3	1210	77.1
1053	28.7	26	1098	*1081*	29.5	*26.5*	1094	37.9	1123	46.9	1184	9.1
1047	19.3	25	1090	*1070*	11.6	*21.6*	1086	11.6	1115	8.6	1176	8.9
1034	70.1	24	1055	*1045*	94.6	*80.5*	1065	78.6	1084	77.3	1161	86.7
1024	32.8	23	1045	*1034*	11.0	*30.0*	1052	6.2	1070	8.5	1143	76.5
1008	193.0	22	1033	*1018*	139.1	*156.0*	1045	107.7	1058	114.7	1130	18.5
989	75.3	21	1013	*1002*	72.1	*85.9*	1014	80.8	1037	64.9	1102	121.8
952	3.5											
932	106.0	20	951	*938*	186.3	*68.9*	964	189.3	980	154.3	1061	137.5
922	224.0	19	941	*927*	90.9	*201.9*	947	66.0	964	87.2	1025	101.2
886[d]	56.1											
		18	902	*891*	101.3	*52.9*	916	105.7	924	113.8	989	62.6
883[d]	139.0											
874	103.0	17	896	*885*	85.8	*199.4*	897	53.8	913	59.4	973	30.1
861	4.2											
847	19.2	16	859	*851*	16.5	*13.7*	868	12.3	885	29.3	928	16.3
821	18.6	15	832	*823*	16.8	*14.5*	841	20.1	859	13.7	895	27.7
807*	0.2											
791*	13.6	14	804	*794*	10.7	*7.2*	812	14.7	826	16.0	869	10.0
752*	1.6	13	767	*763*	0.4	*1.5*	769	1.2	777	17.6	839	0.1
741*	37.2	12	757	*747*	21.9	*28.3*	760	17.1	770	3.5	823	16.9
726*	2.9											
664	2.6	11	667	*664*	1.4	*1.4*	670	1.7	686	2.9	720	5.5
614	42.3	10	623	*622*	28.7	*26.3*	621	27.0	632	32.6	679	45.2
560	0.4											
515	<1.0											
495	18.5	9	499	*498*	10.8	*10.1*	500	12.1	504	16.6	539	11.4
459	57.2	8	460	*460*	38.8	*38.2*	459	38.0	470	37.8	497	49.0
427	40.3	7	433	*432*	40.7	*36.8*	431	41.6	437	43.9	465	29.1
380												
356		6	360	*360*	56.4	*61.1*	359	55.5	363	67.3	388	71.9
329		5	333	*333*	12.6	*15.0*	332	14.1	337	17.1	357	19.7
262		4	262	*256*	0.4	*0.2*	262	0.6	281	0.1	280	0.3
210		3	207	*205*	3.7	*2.7*	206	4.5	218	3.4	223	2.2
		2	157	*150*	3.7	*15.2*	158	2.4	168	5.9	169	12.7
154												
		1	145	*138*	32.1	*25.7*	147	33.5	158	36.6	156	28.5

[a] ν in cm^{-1}; D in 10^{-40} esu^2 cm^2. [b] From IR spectra of CCl_4 or CS_2 solutions of racemic **8** above 400 cm^{-1} and IR spectra of gaseous **8** below 400 cm^{-1}. Parameters from CS_2 solutions are asterisked. The frequency of fundamental 4 is obtained from the experimental Raman spectrum. [c] All calculations use the 6-31G* basis set, except numbers in italic type which have been obtained using the TZ2P basis set. [d] From deconvolved spectra.

Of the modes above 1300 cm^{-1}, VCD is clearly observed for modes 40−42, 44, and 45. For modes 39 and 40, bisignate VCD is predicted by both functionals; the negative VCD of mode 40 is preponderant in both calculations. The observed negative VCD at 1333 cm^{-1} (Table 4) is assignable to mode 40; the VCD of mode 39 is not observed. Both functionals

predict positive VCD for mode 41, as observed. In contrast, B3LYP and B3PW91 predict positive and negative VCD for mode 42, respectively. Negative VCD, assignable to mode 42, is observed. For modes 43−45, both functionals predict a positive-positive-negative VCD sign pattern, in agreement with experiment. The predicted VCD of modes 46−52 is very weak; VCD for these modes is not clearly detectable.

***endo*-5,7-Dimethyl-6,8-dioxabicyclo[3.2.1]octane (5).** The VCD of fundamentals 18−20, 23−32, 35, 36, 38, 39, and 41 is clearly observed. For all of these modes excepting 19 and 23 the B3LYP and B3PW91 predictions are qualitatively identical and in excellent agreement with experiment. B3LYP and B3PW91 predict negative and positive VCD for mode 19, respectively; the experimental VCD is negative. For mode 23 negative and positive VCD are predicted by B3LYP and B3PW91; the experimental VCD is negative. Both functionals predict positive VCD for the nearly degenerate modes 21 and 22, consistent with the single positive band in the experimental spectrum. Both functionals predict negative VCD for the nearly degenerate modes 33 and 34, consistent with the single negative band in the experimental spectrum. Both functionals predict bisignate VCD for modes 37 and 38, the positive VCD of mode 38 preponderating. Mode 38 is clearly observed; mode 37 is not. For modes 39−41, both functionals predict a negative-negative-positive sign pattern. Experimentally, only the VCD of modes 39 and 41 is clearly observed. The two functionals predict very similar VCD for modes 42−45; only mode 44 is observed experimentally. For modes 46−52, significant VCD is predicted only for mode 52. The positive observed VCD agrees with the calculations. The VCD features between modes 44 and 52 are not easily assignable and their origin is unclear.

1,5-Dimethyl-6,8-dioxabicyclo[3.2.1]octane (6). The VCD of fundamentals 18, 21−25, 27−32, 35−39, 41, 42, and 52 is clearly observed. For all of these modes excepting 24, 27−29, and 42, B3LYP and B3PW91 predictions are qualitatively identical and in good agreement with experiment. B3LYP and B3PW91 predict very weak positive and negative VCD for mode 24; the experimental VCD is weak and negative. B3LYP and B3PW91 predict very different VCD spectra for modes 27−29. As with the absorption spectrum, the B3LYP calculation is in better agreement with experiment. However, the relative VCD intensities of modes 27 and 28 are poorly predicted by B3LYP. Both B3LYP and B3PW91 predict negative VCD for mode 42 while the observed VCD is positive. Modes 33/34 are unresolved, together giving large positive VCD. B3LYP and B3PW91 predictions for these modes are quite different, with modes 33 and 34 predominating, respectively. The breadth of the observed band suggests that both modes in fact contribute significantly to the observed VCD. The VCD of modes 19, 20, 26, and 43−51 is not clearly observed. The VCD features observed in the regions where modes 43/44 and modes 50/51 absorb are neither large nor in agreement with calculation; their assignment is uncertain.

Frequencies, dipole strengths, and rotational strengths predicted using MP2 HFFs, MP2 APTs, and semi-MP2 AATs for **2**−**8** are given in Tables 2−8. Absorption and VCD spectra predicted thence are given in Figures 2−8. Overall, MP2 spectra are qualitatively very similar to the DFT spectra; differences are comparable in magnitude to the differences between the B3LYP and B3PW91 spectra. Differences between MP2 and DFT VCD spectra are generally larger than differences in absorption spectra. In part, this can be attributed to the difference in extent to which correlation is included in the AATs. With the exceptions noted below, the MP2 calculations uniformly confirm the assignments of fundamentals based on the DFT calculations.

In the case of **2**, in comparison to the DFT calculations, we note that the VCD of mode 20 is opposite in sign and the VCD of modes 26, 27, and 29 are much smaller in magnitude; the DFT calculations are in uniformly better agreement with experiment. In the case of **3**, the VCD of mode 26 is substantially different and in worse agreement with experiment. The VCD of modes 32−40 differs considerably in detail also, especially for modes 35−37; in this region the VCD is complex and it is difficult to define which calculation is superior. In the case of **4**, we note that for mode 25 the MP2 VCD is similar to the B3LYP prediction, while for modes 27−29 the MP2 calculation reproduces the sign pattern of the B3PW91, and not the B3LYP, calculation. In the case of **5**, the VCD of modes 37/38 is predicted to be bisignate, with mode 37 possessing the larger intensity of positive sign, opposite to the DFT predictions. Here, assignment based on the MP2 calculation leads to a different outcome. In the case of **6**, the MP2 absorption and VCD of modes 26−29 are similar to the predictions of the B3LYP calculation, which differs substantially from the B3PW91 calculation, and are in comparable agreement with experiment.

Frequencies, dipole strengths, and rotational strengths predicted using HF/SCF HFFs, APTs, and ATTs are also given in Tables 2−8. Absorption and VCD spectra predicted thence are also given in Figures 2−8. Overall, HF/SCF spectra are extremely different from DFT spectra, from MP2 spectra, and from experimental spectra with respect to patterns of frequencies and intensities. On the basis of the HF/SCF calculations, the experimental absorption and VCD spectra cannot be convincingly assigned.

We have examined the basis set dependence of predicted absorption and VCD spectra in the case of **3** and **8**. Frequencies, dipole strengths, and rotational strengths calculated using the TZ2P basis set (369 basis functions) are given in Tables 3 and 8. Spectra derived thence are given in Figures 3 and 8. In the case of the absorption spectrum of **3**, qualitative changes with basis set are most apparent for modes 16−19 and 26. Agreement with experiment is not substantially different. In the case of the VCD spectrum, the signs of the VCD of modes 24−26, 31−34, and 39−41 differ. For modes 24, 33, and 40 agreement with experiment is superior for the larger basis set. The negative VCD of the unresolved modes 25/26 is assigned by the TZ2P calculation to mode 26, not mode 25 as in the 6-31G* calculation. In the case of the absorption spectrum of **8**, changes are most noticeable for modes 17−20. The TZ2P calculation is in better agreement with experiment.

Quantitative comparison of calculated and experimental frequencies for **2**−**8** is shown in Figure 9. With the exception of modes below 300 cm^{-1}, for both functionals DFT frequencies are greater than experimental frequencies. The percentage deviations lie in the range 0−6%. The variation in percentage deviation with frequency is fairly monotonic, increasing with increasing frequency. Below 300 cm^{-1} percentage deviations are both positive and negative and exhibit more scatter; however, absolute deviations are uniformly small. For all modes compared in Figure 9 the average absolute percentage deviations of calculated and experimental frequencies are 2.7% and 2.9% for the B3LYP and B3PW91 functionals, respectively. MP2 frequencies are uniformly greater than experimental frequencies. Above 300 cm^{-1} percentage deviations also increase with increasing frequency. Percentage deviations lie in the range 0−9%, larger than for DFT frequencies. For all modes compared in Figure 9 the average absolute percentage deviation

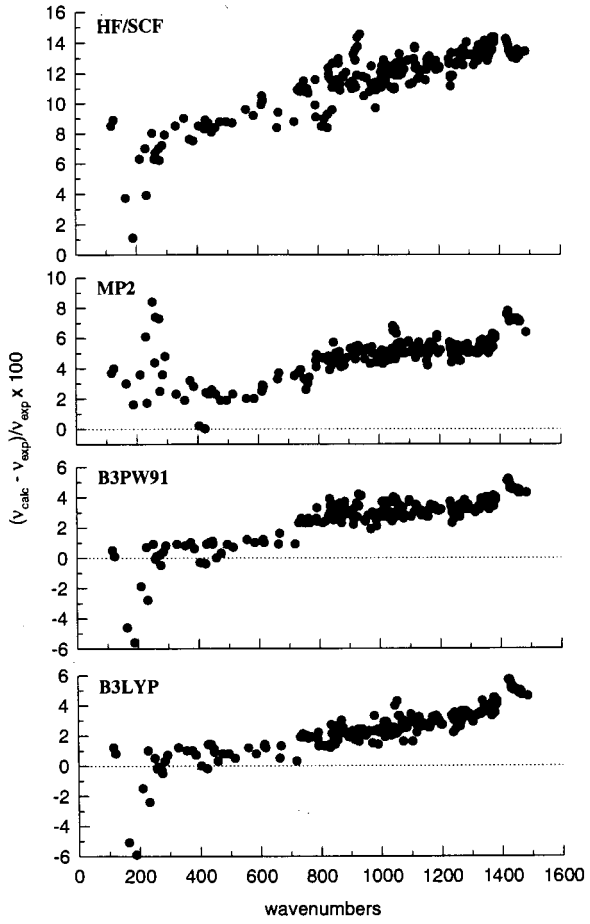

Figure 9. Comparison of calculated and experimental frequencies for **2**−**8**. Modes included (excluded) are as follows: **2**, 1−45 (34, 36, 44); **3**, 1−45 (2, 3, 5, 6, 25, 26, 34, 35, 43); **4**, 18−43 (39, 40); **5**, 18−52 (21, 22, 37, 38, 40, 41, 46−50); **6**, 18−46 (19, 20, 26−28, 33, 34); **7**, 1−45 (17, 18); and **8**, 1−45 (1, 2, 18, 36, 39).

is 4.9%. HF/SCF frequencies are also uniformly greater than experimental frequencies. However, percentage deviations are much larger than for DFT and MP2 frequencies, lying in the range 0−15%. For all modes compared in Figure 9 the average absolute percentage deviation is 11.7%.

Comparison of calculated and experimental dipole strengths for **2**, **3**, **7**, and **8** is shown in Figure 10. Agreement is clearly best for the DFT calculations. MP2 calculations exhibit significantly greater divergence from experiment. HF/SCF dipole strengths exhibit very little correlation with experiment. For the modes compared in Figure 10 the average absolute percentage deviations are 42%, 43%, 52%, and 109% for the B3LYP, B3PW91, MP2, and HF/SCF calculations.

The results shown in Figures 9 and 10 confirm our prior conclusions that B3LYP and B3PW91 DFT calculations are of very similar overall accuracy, that MP2 calculations are somewhat less accurate than DFT calculations, and that HF/SCF calculations are of greatly inferior accuracy.

Discussion

Comparison of the observed mid- and far-IR absorption spectra of **2**−**8** to the predictions of DFT, using the hybrid functionals B3LYP and B3PW91 and the 6-31G* basis set, provides a convincing assignment of a large fraction of the fundamentals of these seven molecules occurring in this spectral region. Fundamentals are not firmly assigned when (a) unresolved from adjacent modes or (b) very weak. The majority

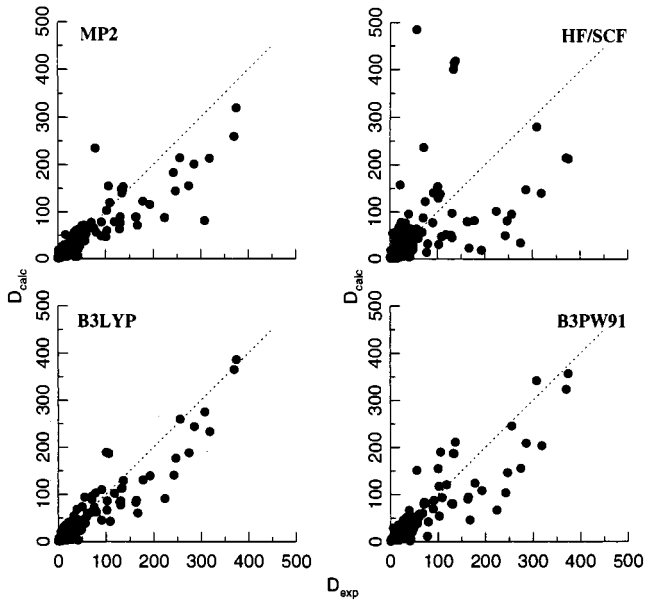

Figure 10. Comparison of calculated and experimental dipole strengths for **2**, **3**, **7**, and **8**. *D* values are in 10^{-40} esu^2 cm^2. Modes are as in Figure 9.

of unresolved modes lie above ∼1300 cm^{-1}. The functionals B3LYP and B3PW91 yield qualitatively similar spectra and, with very few exceptions, identical spectral assignments. The largest differences are in the relative intensities of modes lying very close in frequency. We have made no attempt to assign those observed bands which cannot be assigned as fundamentals. They are very few in number. They are either combination/overtone nonfundamentals or impurity bands.

VCD is observed for a large number of the fundamentals of **2**−**6** lying in the spectral range above ∼800 cm^{-1}, the lower frequency limit of the VCD instrumentation. (The VCD of **7** and **8** was not studied.) Since the signal-to-noise ratio and resolution of the VCD spectra are both inferior to those of the absorption spectra, it is more difficult to observe weak VCD and poorly resolved VCD. In addition, VCD spectra are subject to the incursion of artifacts, especially since they were obtained using single enantiomers. Nevertheless, overall signs and intensities are in good agreement with the predictions of DFT/6-31G* B3LYP and B3PW91 calculations. The principal discrepancies occur for those close-lying modes whose relative VCD intensities differ significantly in the B3LYP and B3PW91 calculations. Where the VCD of two modes which are unresolved in the absorption spectrum is of opposite sign and both modes exhibit significant VCD intensity, the VCD spectrum permits the presence of both modes to be confirmed, adding to the security of the assignment arrived at using the absorption spectrum alone.

The quantitative comparison of observed and predicted fundamental frequencies provides further support for our assignments. Calculated frequencies are greater than experimental frequencies, with the exception of modes in the far-IR, due to (a) calculational error and (b) anharmonicity. For DFT/6-31G* calculations using hybrid functionals these two contributions are comparable in magnitude and together yield differences of up to ∼6%.[21] Our results for **2**−**8**, plotted in Figure 9, are consistent with these expectations. Percentage differences of calculated from experimental frequencies vary more-or-less smoothly with frequency (except in the far IR). Significantly erroneous assignments would lead to greater deviations in this plot.

The use of absorption intensities, in addition to absorption frequencies, is an important component of the assignment of the fundamentals of **2**−**8**. The accuracy of predicted intensities has been examined in the case of **2**, **3**, **7**, and **8** by comparison to experimental intensities. As seen in Figure 10, while there is greater scatter than when frequencies are compared, calculated and experimental intensities vary in parallel, supporting the qualitative use of absorption intensities in spectral assignment.

We have previously assigned the mid- and far-IR fundamentals of **1** using DFT calculations of its absorption and VCD spectra.[5] In addition, analogous studies of the monoterpenes, camphor (**9**),[7] fenchone (**10**),[7] and α-pinene (**11**)[8] have recently been reported. Our results for **2**−**8** parallel those obtained previously in all respects. In the prior studies of **1** and **9**−**11**, calculations were carried out using both 6-31G* and TZ2P basis sets. Although TZ2P calculations are undoubtedly more accurate, the qualitative differences from 6-31G* results are small. In this work, we have carried out TZ2P calculations for **3** and **8**. Again, the spectra predicted differ very little from the 6-31G* spectra and do not lead to changes in assignments. As a result, TZ2P calculations were not carried out for **2** and **4**−**7**.

The DFT calculations reported here use DFT HFFs, APTs, and AATs calculated using nuclear position- and magnetic field-dependent basis sets. As a result, APTs and AATs are of equivalent accuracy as, accordingly, are dipole and rotational strengths. For comparison to the DFT results, we have also carried out MP2 and HF/SCF calculations in parallel. The MP2 calculations use MP2 HFFs and APTs but "semi-MP2" AATs. Rotational strengths are thus intrinsically less accurate than dipole strengths. The HF/SCF calculations use HF/SCF HFFs, APTs, and AATs and, like the DFT calculations, predict dipole and rotational strengths of equivalent accuracy. MP2 absorption and VCD spectra of **2**−**8** are overall very similar to the DFT spectra, consistent with the well-known similarity in accuracy of DFT and MP2 predictions (when hybrid functionals are used for DFT). On the basis of the comparison of calculated and observed frequencies (Figure 9), the DFT calculations are clearly more accurate, consistent with prior comparisons.[21] HF/SCF absorption and VCD spectra in contrast are very different from the DFT and MP2 spectra and are in much worse agreement with experiment. This is attributable to the absence of correlation in the HF/SCF method, leading to a substantially lower accuracy in predictions. Predicted frequencies differ from experimental frequencies by much larger percentages than do DFT and MP2 frequencies (Figure 9). The errors in the HFFs responsible for this also lead to much larger errors in vibrational normal coordinates and, hence, in absorption and VCD intensities (Figure 10). On the basis of the HF/SCF calculations alone a convincing assignment of the spectra of **2**−**8** is not possible. Our MP2 and HF/SCF results for **2**−**8** parallel those obtained previously for **1** and **9**−**11**.

The VCD spectra of **2**−**6** were measured for enantiomers whose absolute configurations had been previously established.[11] In the cases of **2**−**4** and **6**, absolute configurations were determined by synthesis from precursors of known configuration. In the case of **5**, it was assumed that the relationship between the sign of $[\alpha]_D$ and the absolute configurations at positions 1 and 5 is identical to that of **2**−**4** and **6**. The agreement between calculated and observed VCD signs for the vast majority of fundamentals whose VCD is clearly identifiable confirms the previously determined absolute configurations, including that of **5**.

We have also assumed throughout that **2**−**8** exist essentially exclusively in the conformation of the parent molecule, **1**, in which the six-membered ring possesses a chair conformation and the seven-membered ring possesses a boat conformation;[15,22−24] i.e., that the alternative conformation in which the six-membered ring possesses a boat conformation is sufficiently higher in energy to be negligibly populated at room temperature. This assumption is strongly supported by the agreement between predicted and observed absorption and VCD spectra. In addition, in the case of **6**, calculation for the alternative conformer at the DFT/6-31G*/B3LYP level finds an energy difference of 4.4 kcal/mol, identical to that in **1**, showing that the relative energies of the two conformers are insensitive to methyl substitution.

Conclusion

This work is an extension of prior studies of 6,8-dioxabicyclo-[3.2.1]octane (**1**) and its derivatives using vibrational spectroscopy.[5,14,15,20,22−26] These studies have been undertaken with the goal of evaluating the capabilities of current computational methods in predicting the vibrational spectra of organic molecules of medium size, and, hence, their utility in the elucidation of molecular structure and stereochemistry. In this work we have documented the impressive accuracy of DFT in predicting the unpolarized absorption and VCD spectra of seven derivatives of **1**. It is clear that vibrational spectroscopy in combination with DFT calculations now provides a useful tool in determining the molecular stereochemistry of medium-sized organic molecules. Future developments in density functionals, in computational efficiency (such as "linear scaling" techniques), and in computational hardware should further enhance the accuracy and practicability, and hence utility, of DFT calculations in the near future.

Acknowledgment. We are grateful to Drs. M. J. Frisch and J. R. Cheeseman for the GAUSSIAN development code[16] and for helpful discussions. This work was supported by NSF, NIH, the San Diego Supercomputer Center, and NSERCC.

References and Notes

(1) Kinzer, G. W.; Fentiman, A. F.; Page, T. F.; Foltz, R. L.; Vite, J. P.; Pitman, G. B. *Nature* **1969**, *221*, 477.

(2) *Chemical Applications of Density Functional Theory*; ACS Symposium Series 629; Laird, B. B., Ross, R. B., Ziegler, T., Eds.; American Chemical Society: Washington, DC, 1996.

(3) Johnson, B. G.; Frisch, M. J. *Chem. Phys. Lett.* **1993**, *216*, 133; *J. Chem. Phys.* **1994**, *100*, 7429.

(4) Cheeseman, J. R.; Frisch, M. J.; Devlin, F. J.; Stephens, P. J. *Chem. Phys. Lett.* **1996**, *252*, 211.

(5) Stephens, P. J.; Ashvar, C. S.; Devlin, F. J.; Cheeseman, J. R.; Frisch, M. J. *Mol. Phys.* **1996**, *89*, 579.

(6) Devlin, F. J.; Stephens, P. J.; Cheeseman, J. R.; Frisch, M. J. *J. Am. Chem. Soc.* **1996**, *118*, 6327.

(7) Devlin, F. J.; Stephens, P. J.; Cheeseman, J. R.; Frisch, M. J. *J. Phys. Chem.* **1997**, *101*, 6322.

(8) Devlin, F. J.; Stephens, P. J.; Cheeseman, J. R.; Frisch, M. J. *J. Phys. Chem.* **1997**, *101*, 9912.

(9) Becke, A. D. *J. Chem. Phys.* **1993**, *98*, 1372, 5648.

(10) Stephens, P. J.; Devlin, F. J.; Chabalowski, C. F.; Frisch, M. J. *J. Phys. Chem.* **1994**, *98*, 11623.

(11) Ibrahim, N.; Eggimann, T.; Dixon, E. A.; Wieser, H. E. *Tetrahedron* **1990**, *46*, 1503.

(12) Shaw, R. A.; Ibrahim, N.; Wieser, H. *J. Phys. Chem.* **1990**, *94*, 125.

(13) Eggimann, T. Ph.D. Thesis, University of Calgary, Alberta, Canada, 1991.

(14) Bak, K. L.; Devlin, F. J.; Ashvar, C. S.; Taylor, P. R.; Frisch, M. J.; Stephens, P. J. *J. Phys. Chem.* **1995**, *99*, 14918.

(15) Ashvar, C. S.; Devlin, F. J.; Bak, K. L.; Taylor, P. R.; Stephens, P. J. *J. Phys. Chem.* **1996**, *100*, 9262.

(16) GAUSSIAN 92; GAUSSIAN 92/DFT; GAUSSIAN 94; GAUSSIAN 95 (Development Version); Gaussian Inc.: Pittsburgh, PA.

(17) SIRIUS: Jensen, H. J. Aa.; Aagren, H.; Olsen, J. ABACUS: Helgaker, T.; Bak, K. L.; Jensen, H. J. Aa.; Jorgensen, P.; Kobayashi, R.; Koch, H.; Mikkelsen, K.; Olsen, J.; Ruud, K.; Taylor, P. R.; Vahtras, O.

(18) Stephens, P. J.; Jalkanen, K. J.; Amos, R. D.; Lazzeretti, P.; Zanasi, R. *J. Phys. Chem.* **1990**, *94*, 1811.

(19) Kawiecki, R. W.; Devlin, F. J.; Stephens, P. J.; Amos, R. D. *J. Phys. Chem.* **1981**, *95*, 9817.

(20) Smithson, T. L. Ph.D. Thesis, University of Calgary, Alberta, Canada, 1982.

(21) Finley, J. W.; Stephens, P. J. *THEOCHEM, J. Mol. Struct.* **1995**, *357*, 225.

(22) Eggimann, T.; Shaw, R. A.; Wieser, H. *J. Phys. Chem.* **1991**, *95*, 591.

(23) Eggimann, T.; Ibrahim, N.; Shaw, R. A.; Wieser, H. *Can. J. Chem.* **1993**, *71*, 578.

(24) Stephens, P. J.; Devlin, F. J.; Ashvar, C. S.; Chabalowski, C. F.; Frisch, M. J. *Faraday Discuss.* **1994**, *99*, 103.

(25) Shaw, R. A.; Ibrahim, N.; Wieser, H. *Tetrahedron Lett.* **1988**, *29*, 745.

(26) Eggimann, T.; Wieser, H. *Proc. SPIE—Int. Soc. Opt. Eng.* **1991**, *1575*, 412.